







# Subaqueous acoustic pressure system based one day heterotypic pseudo-islet spheroid formation with adipose derived stem cells for graft survival-related function enhancement

Jiyu Hyun<sup>a,1</sup>, Junhyeung Park<sup>b,1</sup> , Jihun Song<sup>c,d</sup>, Chaerim Yoo<sup>e</sup>, Seonmi Jang<sup>e</sup>, Sang Yoon Lee<sup>a</sup>, Jiseon An<sup>a</sup>, Hyun Su Park<sup>a</sup>, Seunghyuk Jung<sup>f</sup>, Dasom Kong<sup>g</sup>, Ji Hyeon Cho<sup>b</sup>, Tae Il Lee<sup>h</sup>, Ki Dong Park<sup>g</sup>, Gwang-Bum Im<sup>a,i</sup> , Jee-Heon Jeong<sup>b,\*</sup>, Hyun-Ji Park<sup>g,j,\*\*</sup> , Dong Yun Lee<sup>e,k,\*\*\*</sup> , Suk Ho Bhang<sup>a,\*\*\*\*</sup>

<sup>a</sup> School of Chemical Engineering, Sungkyunkwan University, Suwon, 16419, Republic of Korea

<sup>b</sup> Department of Precision Medicine, School of Medicine, Sungkyunkwan University, Suwon, 16419, Republic of Korea

<sup>c</sup> Biomedical Research Center, Korea University Guro Hospital, Seoul, Republic of Korea

<sup>d</sup> Department of Biomedical Informatics, Korea University College of Medicine, Seoul, Republic of Korea

<sup>e</sup> Department of Bioengineering, College of Engineering, Hanyang University, Seoul, 04763, Republic of Korea

<sup>f</sup> Department of Applied Chemistry & Biological Engineering, Ajou University, Suwon, 16499, Republic of Korea

<sup>g</sup> Department of Molecular Science and Technology, Ajou University, Suwon, 16499, Republic of Korea

<sup>h</sup> Department of Materials Science and Engineering, Gachon University, Seong-nam, 13120, Republic of Korea

<sup>i</sup> Department of Cardiac Surgery, Boston Children's Hospital, Boston, MA, USA

<sup>j</sup> Advanced College of Bio-Convergence Engineering, Ajou University, Suwon, 16499, Republic of Korea

<sup>k</sup> Elixir Pharmatech Inc., Seoul, 04763, Republic of Korea

## ARTICLE INFO

### Keywords:

Acoustic levitation  
Adipose-derived stem cell  
Cell culture system  
Pancreatic islet  
Pseudo islet  
Type 1 diabetes mellitus

## ABSTRACT

To overcome Type 1 diabetes mellitus (T1DM), which can cause hyperglycemia due to diminished insulin secretion of  $\beta$ -cell function, islet transplantation has been developed with various strategies including pseudo-islet. However, conventional pseudo-islet formation techniques combining with other cells depend on natural cellular aggregation, which requires at least 5 days to form and even show segregation of distinct cell types, leading to diminished cell viability and function. Herein, we applied a subaqueous free-standing 3D cell culture (FS) device, which can reduce the spheroid formation time by trapped cell in nodes of acoustic standing wave. Briefly, Culturing with adipose-derived stem cells (ADSCs) to form heterotypic pseudo-islet (Hislet) in FS device dramatically reduced formation time less than one day. Hislet demonstrated enhancement of cell viability than conventional pseudo-islet formation method. Additionally, ADSCs combined Hislet proved strong secretion of various paracrine factors. Also results showed significantly increased angiogenesis effect and immunomodulation effect for various type of immune cells in Hislet compared to islet, which can enhance transplantation survival. Furthermore, Hislet validated glucose-regulating capacity and enhanced angiogenesis effect *in vivo* T1DM model. Throughout this study, we propose a novel strategy for forming Hislet that can overcome the limitations of conventional Islet and pseudo-islet for T1DM.

Peer review under the responsibility of editorial board of Bioactive Materials.

\* Corresponding author. Department of Precision Medicine, School of Medicine, Sungkyunkwan University, Suwon 16419, Republic of Korea.

\*\* Corresponding author. Department of Molecular Science and Technology, Ajou University, Suwon, 16499, Republic of Korea.

\*\*\* Corresponding author. Department of Bioengineering, College of Engineering, Hanyang University, Seoul, 04763, Republic of Korea.

\*\*\*\* Corresponding author. School of Chemical Engineering, Sungkyunkwan University, Suwon 16419, Republic of Korea.

E-mail addresses: [jeeheon@skku.edu](mailto:jeeheon@skku.edu) (J.-H. Jeong), [hyunjiipark@ajou.ac.kr](mailto:hyunjiipark@ajou.ac.kr) (H.-J. Park), [dongyunlee@hanyang.ac.kr](mailto:dongyunlee@hanyang.ac.kr) (D.Y. Lee), [sukhobhang@skku.edu](mailto:sukhobhang@skku.edu) (S.H. Bhang).

<sup>1</sup> These authors contributed equally to this work.

<https://doi.org/10.1016/j.bioactmat.2025.05.005>

Received 25 November 2024; Received in revised form 10 April 2025; Accepted 7 May 2025

2452-199X/© 2025 The Authors. Publishing services by Elsevier B.V. on behalf of KeAi Communications Co. Ltd. This is an open access article under the CC BY-NC-ND license (<http://creativecommons.org/licenses/by-nc-nd/4.0/>).

## 1. Introduction

Type 1 diabetes mellitus (T1DM) is a chronic autoimmune disease characterized by insulin deficiency due to reduced  $\beta$ -cell function, leading to failure in controlling blood glucose level and resulting in hyperglycemia [1]. Since endogenous insulin production is insufficient to maintain blood glucose homeostasis in T1DM patients, they must rely on exogenous insulin in various method to control the blood glucose level [2,3]. To overcome the dependence on exogenous insulin injections, pancreatic islet transplantation has been used as a therapy to restore patients' ability to produce their own insulin [4]. However, naïve islet (Islet) transplantation had shown the low graft survival rate due to various factors, such as 1) transplant rejection by the host's immune cells, 2) cell death caused by necrotic inner cores of the large-diameter pancreatic islet, and 3) poor blood, nutrient, and oxygen supply due to the failure to form new blood vessels after transplantation [5–7]. To address these limitations, various methods combining scaffold and material have been developed to improve transplanted islet survival by protecting from immune cells or enhance neovascularization [8–12]. While effective, these strategies still require the use of non-human-derived foreign materials, which may pose immunogenic risks [13]. Additionally, pancreatic islet vary in size (50–400  $\mu\text{m}$ ), and islet with large diameters ( $>150 \mu\text{m}$ ) are more vulnerable during transplantation due to necrotic cores [14]. In short, scaffolds and materials-based strategies have not been able to resolve this issue.

To improve the graft-survival without using foreign materials, pseudo-islet (p-islet) formation techniques have been developed by dissociating pancreatic islet and then re-aggregating them with endothelial cells or mesenchymal stem cells (MSCs) to control their size and enhance vascularization [15–18]. By controlling the diameter of the aggregate less than 150  $\mu\text{m}$ , the p-islet exhibit enhanced glucose-responsive insulin secretion, leading to better therapeutic effects for T1DM by enhancing graft survival [19]. The incorporation of MSCs in islet transplantation has demonstrated several benefits. MSCs facilitate neovascularization, mitigating graft rejection through growth factor and cytokine secretion which is crucial for the long-term viability of transplanted Islet [20,21]. Furthermore, the paracrine effects of MSCs, mediated through the secretion of various growth factors and cytokines, contribute to improved islet survival and function [22]. These trophic factors create a supportive microenvironment, enhancing  $\beta$ -cell proliferation and insulin secretion [23]. Collectively, these mechanisms synergistically augment the overall therapeutic efficacy of islet transplantation, potentially leading to improved clinical outcomes in the treatment of diabetes.

While p-islets had advantages in size control and enhanced functionality when combined with other cells containing MSCs, the process is labor-intensive and requires long formation time (at least 5 days) which can reduce cell viability and efficiency caused by cell loss [24]. Furthermore, the formation of pseudo-islet through the amalgamation of heterotypic cellular populations have revealed an inherent tendency towards cellular segregation [24]. This phenomenon, characterized by the spatial separation of distinct cell types within the pseudo-islet structure, presents a significant challenge in maintaining the desired cellular composition and architecture [25]. Such segregation may potentially compromise the functional integrity and long-term stability of the engineered pseudo-islet, necessitating the development of advanced strategies to mitigate this issue and ensure sustained cellular integration. In this context, new approaches are required to enhance the therapeutic efficacy of p-islet.

In our previous study, we have designed a subaqueous free-standing 3D cell culture (FS) device based on acoustic standing waves in the vertical direction, which can form cell spheroids in relatively short time compared to conventional 3D culture methods [26]. Applying the FS device to mesenchymal stem cell culture resulted in a 4-fold faster spheroid formation time compared to conventional methods. Thus, we aim to enhance p-islet formation by co-culturing pancreatic islet cells

with adipose-derived mesenchymal stem cells (ADSCs) using the FS device. ADSCs, which can be obtained from adipose tissues, have high therapeutic potential in inducing angiogenesis and immunomodulation due to their strong secretion of paracrine factors and cytokines [27–29]. After spheroid formation, ADSCs show upregulated angiogenic properties caused by hypoxic cores within the spheroids that increase HIF-1 $\alpha$  expression, which in turn upregulates the secretion of angiogenic factors through HIF-1 $\alpha$ -mediated cell signaling [30,31]. This mechanism also allows ADSCs and adjacent cells to exhibit tolerance to hypoxic conditions [32,33]. Moreover, ADSCs induce high extracellular matrix (ECM) expression, enhancing stability, reducing the time required for spheroid formation, and therefore strengthening cell function [34,35]. Specifically, our approach seeks to create multifunctional p-islet that exhibit improved angiogenesis, immunomodulation, and insulin secretion capabilities, while significantly reducing the formation time from days to hours through the efficient use of the FS device.

In this study, we present a highly functional heterotypic pseudo-islet (Hislet) composed of ADSCs and pancreatic islet cells formed in a short time using the FS device. Remarkably, only 8 h were required to form Hislet by using FS device, and an additional 12-hr culture period strengthened their stability. Hislet had an average diameter of 105  $\mu\text{m}$  and showed comparable cell viability to freshly isolated pancreatic islets, addressing the problem of nutrient and oxygen deficiency in the cores of large-diameter pancreatic islet. RNA sequencing result supported that Hislet showed enhanced angiogenesis, immunomodulation, and insulin secretion compared to Islet without ADSCs, due to their increased ECM expression and secretion of various paracrine factors crucial for the survival of transplanted cells [36]. Additionally, they maintained glucose-dependent insulin secretion properties essential for treating T1DM and showed immunomodulation effect for various immune cells which is crucial for graft survival. Lastly, *in vivo* T1DM models demonstrated that Hislet effectively regulates blood glucose levels.

## 2. Materials and methods

### 2.1. Cell culture

Rat ADSCs was purchased from iXCells Biotechnologies (San Diego, CA, USA). Cells were cultured in Dulbecco's Modified Eagle's Medium/Nutrient Mixture F-12 (DMEM/F-12; Gibco BRL, Gaithersburg, Maryland, USA) supplemented with 10 % (v/v) fetal bovine serum (FBS, Gibco BRL) and 1 % (v/v) penicillin/streptomycin (PS, Gibco BRL). The cells were incubated at 37 °C and 5 % CO<sub>2</sub> saturation. The cell culture medium was changed every 2 days. Rat ADSCs within 5 passages were used.

### 2.2. Islet isolation and purification

Pancreatic islets were isolated from male Sprague-Dawley rats (DBL, Chungcheongbuk-do, Republic of Korea) using an enzymatic digestion method. In brief, 10 mL of 0.8 mg/mL collagenase P solution (Roche Diagnostics, GmbH, Mannheim, Germany) was carefully injected into the pancreas through cannulation of the pancreatic duct. The pancreas was subsequently excised and incubated at 37 °C for 18 min. Islets were purified by density gradient centrifugation with a Ficoll Paque PLUS/RPMI-1640 medium gradient. The isolated islets were then manually selected and cultured in RPMI-1640 medium (Sigma Aldrich, St Louis, MO) supplemented with 10 % FBS (Gibco BRL) and 1 % PS (Gibco BRL). All animal experiments were conducted in strict accordance with national guidelines and received approval from the Institutional Animal Care and Use Committee (IACUC) of Sungkyunkwan University, Republic of Korea (SKKUIACUC2023-01-31-1).

### 2.3. Design of FS device

The piezoelectric actuator used in this study was made of lead zirconate titanate and fabricated as a 20 mm in diameter, 1.3 mm thick, round disc with 1800 pF capacitance and 1.6 MHz resonance frequency. The piezoelectric actuator was installed at the bottom of the cell culture vessel, and the reflector was positioned about the upper side. As the sidewall of the cell culture vessel, a borosilicate tube with an outer diameter of 50 mm and a wall thickness of 5 mm was used. Both the top and bottom sides of the vessel tube were plugged in with O-ring sealed actuator and reflector components. In order to control the distance between the actuator and reflector to tune the resonance condition of acoustic waves, the holder of the reflector was designed to be movable. To maintain a temperature of approximately 36 °C in the cell culture vessel, cooling water was circulated through the aluminum frame containing heat sources such as the actuator and the driving circuit.

### 2.4. Spheroid formation using FS device

DMEM/F-12 and RPMI 1640 supplemented with 10 % FBS and 1 % PS were mixed in 1:1 ratio for co-culture media of pancreatic islet cells and rat ADSCs [37]. 150 IEQ were dissociated by treating accutase for 20 min in 37 °C (ThermoFisher, A1110501, Waltham, MA, USA). After pancreatic islets were dissociated to single cells, they were co-cultured with  $2.5 \times 10^5$  rat ADSC cells in FS device with co-culture media. The formed Hislet was easily retrieved from the FS device by turning off the device. After the power was off, the spheroids settled at the bottom and were gently retrieved with a pipette (Supplementary Movie. 1).

### 2.5. Spheroid formation using U-shaped 96-well

Round-bottom 96-well plates (Corning, NY, USA) coated with poly (2-hydroxyethyl methacrylate) were seeded with  $5 \times 10^3$  cells per well, consisting of 1:1 ratio of mixed dissociated pancreatic islet single cells and rat ADSC cells, in co-culture media. Plates were incubated at 37 °C for inducing spheroid formation.

### 2.6. DiI staining

Rat ADSCs cultured on the cell culture plate were treated with DiI (Sigma-Aldrich, St. Louis, MO, USA) mixed with DMEM/F-12 at a ratio of 1:200 for 2 h and then washed twice with PBS. DiI-stained rat ADSCs were used in Hislet formation by using FS device.

### 2.7. Hematoxylin & eosin staining

Pancreatic islet and Hislet were fixed with 4 % formaldehyde for 24 h and immersed with 30 % sucrose for another 24 h. The cells were embedded in optimum cutting temperature (OCT, SciGen Scientific, Gardenas, USA) compound. Next, 10 µm sections were obtained from specimens and stained with H&E.

### 2.8. FDA/EB staining

FDA/EB staining was performed using fluorescein diacetate (FDA, Sigma-Aldrich) and ethidium bromide (EB, Sigma-Aldrich). FDA (green) stains the cytoplasm of viable cells, whereas EB (red) stains the nuclei of nonviable cells. The staining solution was freshly prepared by combining 10 mL of FDA stock solution (1.5 mg/mL of FDA in dimethyl sulfoxide), 5 mL of EB stock solution (1 mg/mL of EB in PBS), and 3 mL of PBS. Pancreatic Islet and Hislet were then incubated with the staining solution for 3 min at 37 °C. After staining, the samples were washed twice with PBS and examined using a fluorescence microscope (DFC 3000 G, Leica, Wetzlar, Germany).

### 2.9. Flow cytometry for cell viability

Pancreatic islet and Hislet were dissociated by accutase (Gibco BRL) treatment for 20 min at room temperature. The cells in each group were centrifuged for 5 min at 250 g. Then, cells were washed twice with cold cell staining buffer (Biolegend, San Diego, CA, USA) and treated with 100 µL of Annexin V binding buffer (Biolegend). After treatment with Annexin V binding buffer, the cells were transferred to test tubes. Annexin V (Biolegend) and 7-aminoactinomycin D (7-AAD, Biolegend) solution were added to the hDFs in the test tubes. Annexin V binds to phosphatidylserine on the external leaflet of the plasma membrane of apoptotic cells, while 7-AAD solution penetrates the nuclear membrane and binds to the DNA of necrotic cells. Next, the test tubes were gently vortexed and incubated for 15 min at room temperature. More Annexin V binding buffer (200 µL) was added to each cell in the test tubes and the cells were analyzed by flow cytometry with a CytoFLEX flow cytometer (Beckman Coulter, Brea, CA, USA).

### 2.10. Apoptotic activity

For apoptotic activity, pancreatic islet and Hislet were fixed with 4 % paraformaldehyde solution and immersed with 30 % sucrose for another 24 h. After fixation, the cells were embedded in OCT compound. OCT block was cut into 10 µm-thick sections at –22 °C. A terminal deoxynucleotide transferase-mediated deoxyuridine triphosphate nick-end labeling (TUNEL) assay was performed using the ApopTag® Fluorescent In Situ Apoptosis Detection Kit (Millipore, Bedford, MA, USA) to examine the apoptotic activity of each group. Following 4,6-diamidino-2-phenylindole (DAPI, Vector Laboratories, Newark, CA, USA) staining, TUNEL-positive fluorescence was measured using a fluorescence microscope (DFC 3000G, Leica).

### 2.11. Immunofluorescence staining

For immunofluorescence staining, pancreatic Islet and Hislet were fixed with 4 % paraformaldehyde solution and immersed with 30 % sucrose for another 24 h. After fixation, samples embedded in the OCT compound were cut into 10-µm-thick sections at –22 °C. Sections were immunofluorescently stained with Ki67 (Abcam, ab16667, 1:250, Cambridge, UK), Collagen1 (Col1, Abcam, ab34710, 1:50), Connexin 43 (Con43, Abcam, ab235585, 1:250), Laminin (Abcam, ab11575, 1:200), E-cadherin (Abcam, ab231303, 1:100), Insulin (Abcam, ab181547, 1:200). Positive signals of each protein were visualized with fluorescein isothiocyanate-conjugated secondary antibodies (Jackson ImmunoResearch Laboratories, West Grove, PA, USA). These sections were then counterstained with DAPI (Vector Laboratories) and examined using a fluorescence microscope (DFC 3000 G, Leica).

### 2.12. Western blot analysis

For Western blot analysis, samples lysed in radio-immunoprecipitation assay (RIPA) buffer (Rockland Immunochemicals Inc., Limerick, PA, USA) buffer. After centrifugation at 10,000 g for 10 min, the supernatant was prepared as a protein extract. Protein concentrations were determined using a Bicinchoninic Acid Assay (BCA assay) (Pierce Biotechnology, Rockford, IL, USA). Equal amounts of protein from each sample were mixed with a sample buffer and subjected to sodium dodecyl sulfate polyacrylamide gel electrophoresis (SDS-PAGE) using a 10 % (v/v) resolving gel. The separated proteins were transferred to immune-blot Polyvinylidene difluoride (PVDF) membranes (Bio-Rad, Hercules, CA, USA). The membranes were blocked with 5 % (w/v) skim milk in Tris-buffered saline (TBS; 50 mM Tris-HCl (pH 7.5), 150 mM NaCl, 2.5 mM KCl) and incubated for 1 h at 25 °C. Then, the membranes were probed overnight at 4 °C with antibodies against glyceraldehyde 3-phosphate dehydrogenase (GAPDH) (Abcam, ab9485, 1:2000, Cambridge, UK), ITGA5 (Abcam, ab179475, 1:1000),

Con43 (Abcam, ab235585, 1:1000), Laminin (Abcam, ab11575, 1:1000), and CD44 (Abcam, ab189524, 1:1000). Thereafter, the membranes were incubated with horseradish peroxidase-conjugated secondary antibody (R&D Systems, Minneapolis, MN, USA, HAF017 for GAPDH, 1:2000 for ITGA5, Con43, Laminin and CD44, 1:1000, Minneapolis, MN, USA) for 1 h at 25 °C, followed by addition of ECL reagent (TransLab, Daejeon, Republic of Korea). The blots were developed in a dark room, and luminescence was recorded using an X-ray blue film (Agfa HealthCare NV, Mortsel, Belgium). Quantification of Western blot was performed by image J analysis (National Institutes of Health, Bethesda, MD, USA).

### 2.13. Quantitative reverse transcription polymerase chain reaction

Quantitative reverse transcription polymerase chain reaction (qRT-PCR) was used to quantify the relative gene expression levels of each experiment. Rat-specific gene primers were used for Islet and Hislet analyses. Total ribonucleic acid (RNA) was extracted from the samples using 1 mL TRIzol reagent (Life Technologies, Inc., Carlsbad, CA, USA) and 200  $\mu$ L chloroform. The lysed samples were centrifuged at 12,000 rpm for 10 min at 4 °C. The RNA pellet was washed with 75 % (v/v) ethanol in water and dried. The samples were then dissolved in RNase-free water. The SsoAdvanced Universal SYBR Green Supermix kit (Bio-Rad) and CFX Connect™ real-time PCR detection system (Bio-Rad) were used for qRT-PCR. Table 1 lists the primers used for qRT-PCR.

### 2.14. Rat cytokine array

Islet and Hislet were cultured in serum-free co-culture media for additional 2 days. After retrieving the conditioned media (CM) from each group, RAT XL cytokine array (ARY030, R&D Systems) was conducted following the manufacturer's protocols. Pixel densities were quantified with Image J software (National Institutes of Health). Signals from duplicated spots were averaged.

### 2.15. Tube formation assay

Human umbilical vein endothelial cells (HUVECs) were purchased from PromoCell (Heidelberg, Germany) and cultured in endothelial cell media (PromoCell) supplemented with Growth Medium SupplementMix (PromoCell) at 37 °C with 5 % CO<sub>2</sub>. The medium was changed every 2 days. Cells within four passages were used in the experiments. Tube formation of HUVECs was conducted using an Angiogenesis assay kit *in vitro* (ab204276; Abcam) following the manufacturer's protocols. The CM extracted from each group was mixed with HUVEC medium at a 1:1 ratio and then used to treat HUVECs cultured on pre-coated Matrigel.

### 2.16. RNA-sequencing

RNA sequencing was performed on Hislet and Islet. Briefly, RNA was isolated using TRIzol reagent (Life Technologies, Inc.). The purified RNA was analyzed for size, quality, and quantity, then cDNA library was constructed using QuantSeq 3' mRNA-seq Library Prep Kit FWD for further sequencing (NextSeq 550, Illumina). All reads were trimmed and mapped using the STAR aligner and data analysis was performed using R. Initially, RNA counts were preprocessed using the *edgeR* package to remove genes with a total RNA counts 0 and those with 0 in more than two samples per group. The RNA counts were then normalized across groups using the trimmed mean of M-values (TMM) method and converted to log2 counts per million (CPM). Principal component analysis (PCA) was conducted to compute principal components and eigenvalues using the *FactoMineR* and *FactoExtra* packages. Library sizes were calculated using R's built-in function. Differential expression analysis between Islet and Hislet was performed using the *dream* function from the *variancePartition* package, which enables empirical Bayesian statistical analysis. Volcano plots were generated to visualize significant differences in gene expression using the *EnhancedVolcano* package. Genes with an absolute log2 fold change greater than 2 and a p-value less than 0.01 were highlighted. Hierarchical clustering heatmaps were then created using the *pheatmap* package to illustrate the expression patterns differentially expressed genes.

### 2.17. Glucose-stimulated insulin secretion

For investigating the responses to varying glucose concentrations, the glucose-stimulated insulin secretion (GSIS) assay was performed. Islet and Hislet were pre-incubated with Krebs Ringer Buffered HEPES (KRBH; pH 7.4) containing 2.8 mM glucose at 37 °C for 30 min. Next, they were cultured in either a low-glucose (2.8 mM) or high-glucose (20.2 mM) buffer for 1 h [38]. The insulin concentrations in the culture buffers were measured by a commercial rat insulin enzyme-linked immunosorbent assay (ELISA) kit (Alpco Diagnostics, Salem, NH, USA). The stimulation index (SI) values were calculated by the following formula: (normalized amount of secreted insulin at high glucose)/(-normalized amount of secreted insulin at low glucose).

### 2.18. Analysis of inducing M2 polarization of M1 macrophage

RAW 264.7 cell lines (ATCC) were cultured with Dulbecco's Modified Eagle Medium (DMEM, Gibco BRL). 1 % (v/v) penicillin-streptomycin (PS, Gibco BRL) and 10 % (v/v) fetal bovine serum (FBS, Gibco BRL) were supplemented. Cells were maintained in a humidified incubator at 37 °C with 5 % CO<sub>2</sub>, and the culture medium was replaced

**Table 1**  
Primer sequences for qRT-PCR.

Gene	Forward	Reverse
Rat GAPDH	AACGACCCCTTCATTGACCTC	CCTTGACTGTCCGTTGAAC
Rat VEGF	TTTCTCCGCTCTGAACAAGGC	TGCAGATCATGCGGATCAAAC
Rat IGF-1	TGGTGGACGCTCTTCAGTTC	AGTGTACTTCCTTCTGAGTCTTGG
Rat Angpt-2	CATGATGTCATCGCCGACT	TCCATGTACAGTAGGCCTTG
Rat FGF2	GATCCCAAGCGGCTCTACTG	TAGTTTGACGTGTGGGTCCG
Rat IL-1	TCTCTCCGCAAGAGACTTCCA	ATACTGGTCTGTTGTGGGTGG
Rat IL-1b	TTACCATGGAACCCGTGTC	GGAGACTGCCATTCTCGAC
Rat IRF1	TGAAGCTGCAACAGATGAGG	AGCAAGTATCCCTTGCCATC
Rat TNF- $\alpha$	AAATGGGCTCCCTCTCATCAGTTC	TCTGCTTGGTGGTTTGTCTACGAC
Rat IL-4	AGGGTGCTTCGCAAAATTTTA	CAGTGTGTGAGCGTGGACT
Rat IL-10	CCTGCTCTTACTGGCTGGAG	TGTCCAGCTGGTCTCTTT
Rat IL-13	TTCCCTGACCAACATCTCCAA	TTGCGGTTACAGAGGCCATG
Rat TGF- $\beta$	GGATCTTGGGTGGAAATGGATTCA	ACACGACAGCAAGGGGAAGCA
Rat PDX1	AAATCCACCAAGCTCACGC	GGTCAAGTTCAACATCACTGCC
Rat HK1	GACCCGAGGCATCTTGA	AGCAGCGCTAATCGGTCACT
Rat GLUT1	TTGACGGCTTCTCCAAGTGAC	CAGAACCAGGAGCAGTGAAG
Rat UCP2	CCAATGTTGCCCGAAATG	CCCGAAGGCAGAGTGAAG



every other day. For M1 polarization, RAW 264.7 cells were treated with lipopolysaccharide (LPS, 1 µg/mL) for 24 h. After inducing M1 polarization, the CM extracted from each group was mixed with DMEM medium at a 1:1 ratio and applied to M1-polarized Raw 264.7 cells for 24 h. Cells were then harvested by scraping, centrifuged (125 RCF, 3 min, 25 °C), and resuspended in cell staining buffer (BioLegend). The suspended cells were incubated in dark for 30 min at room temperature with 100 µL of staining solution containing fluorescein isothiocyanate (FITC)-conjugated anti-mouse CD206 and Brilliant Violet 605-conjugated anti-mouse CD11b antibodies. After staining, 400 µL of cell staining buffer was added to sample, and flow cytometry analysis was performed using a CytoFLEX flow cytometer (Beckman Coulter).

## 2.19. Splenocyte isolation, activation, and co-culture with islet or Hislet

Eight-week-old male C57BL/6 mice were sacrificed, and their spleens were aseptically harvested. The spleens were mechanically dissociated by gently crushing and passing through a sterile 70-µm nylon filter in RPMI-1640 medium (Sigma Aldrich) supplemented with 10 % FBS (Gibco BRL) and 1 % PS (Gibco BRL). To eliminate erythrocytes, the cells were treated with RBC lysis buffer (10 × ; BioLegend) diluted 1:10 in PBS. The remaining cells were washed and resuspended in complete RPMI-1640 medium. Splenocytes were counted using a hemocytometer, and  $1 \times 10^6$  cells were pre-treated with Dynabeads® Mouse T-Activator CD3/CD28 (Gibco) at a 1:1 bead-to-cell ratio for activation prior to co-culture experiments. Islet and Hislet were co-cultured with the activated splenocytes for 2 days in coculture medium.

## 2.20. Peripheral blood mononuclear cell (PBMC) culture, activation, and co-culture experiment

PBMCs from healthy adult donor (age 56; male) were purchased from CGT Global and used for experiments. PBMCs were thawed and subsequently incubated for 2 h at 37 °C in a 5 % CO<sub>2</sub> incubator, followed by activation for 24 h in RPMI 1640 medium (Gibco) supplemented with 10 % FBS (Gibco), GM-CSF (50 ng/mL), IL-4 (50 ng/mL), IL-2 (50 ng/mL), IL-15 (50 ng/mL), and DynaBeads® Human T-Activator CD3/CD28 (Gibco,  $5 \times 10^5$  beads per  $1 \times 10^6$  PBMCs). To assess cytotoxicity,  $1 \times 10^4$  cells of Islet or Hislet (target cells) were plated in 96-well plates, and activated PBMCs (effector cells) were added at different effector-to-target (E:T) cell ratios (1:1, 5:1, and 10:1). After 4 h of incubation in serum-free culture medium, the LDH cytotoxicity assay (Roche Diagnostics, Basel, Switzerland) was performed according to the manufacturer's instructions. Cytotoxicity was calculated as the percentage of LDH release, determined by subtracting the spontaneous LDH release from untreated Islet or Hislet (low control) from the experimental value, and then dividing by the difference between the maximum releasable activity (high control) and the low control. For flow cytometry assay, activated PBMCs were co-cultured with Islet and Hislet for 3 days in a co-culture medium consisting of a 1:1 mixture of islet culture medium and RPMI 1640 supplemented with 10 % FBS. After co-culture, cells were harvested, fixed, and stained with FITC-conjugated antibodies targeting immune cell markers. Antibodies included anti-CD4 (1:100, BD Bioscience, Franklin Lakes, NJ, USA) and anti-CD8 (1:100, BD Bioscience) for CD4<sup>+</sup> T cells and CD8<sup>+</sup> T cells respectively, anti-CD19 (1:250, BD Bioscience) for B cells, and anti-CD56 (1:500, BD Bioscience) for NK cells. Flow cytometry analysis was then performed using a NovoCyte Flow Cytometer (Agilent, Santa Clara, CA, USA), and data were analyzed by manual gating with NovoExpress software (version 1.6.2, Agilent).

## 2.21. Diabetes induction and transplantation

Diabetic Balb/c-nude mice (male, 8 weeks old) were established by intraperitoneal injection of streptozotocin (STZ) solution in 0.1 M of citrate buffer (220 mg/kg, Sigma-Aldrich). Only mice with non-fasting

blood glucose (NBG) levels higher than 300 mg/dL for two consecutive days were considered diabetic. For transplantation, mice were anesthetized via inhalation of isoflurane solution for islet transplantation. The left kidneys were exposed, and pouch was beneath the kidney capsule. Naïve islet (400 IEQ) and Hislet (equivalent to 400 IEQ) were injected slowly into the subcapsular pouch. The functionality of the transplanted islets and Hislets was assessed by regularly monitoring NBG level using commercial glucose meter (Handok, Seoul, Republic of Korea). On day 20 post-transplantation, intraperitoneal glucose tolerance test (IPGTT) was performed after 6 h of fasting. Glucose solution (2.0 g/kg) was injected intraperitoneally, and blood glucose levels were recorded at 0, 5, 10, 15, 30, 60 and 120 min after injection.

## 2.22. Histological assessment

Graft-bearing kidneys were harvested 21 days post-transplantation, fixed in 4 % paraformaldehyde (PFA) for 48 h, and incubated in 30 % sucrose for 48 h. After fixation, samples embedded in the OCT compound were sectioned at 10 µm thickness at −22 °C. For antigen retrieval, slides were treated with proteinase K buffer (0.6 unit/mL in Tris-EDTA pH 8.0 with 0.5 % Triton X-100 in PBS) at 37 °C for 10 min. Sections were incubated in blocking solution (0.3 % Triton X-100, 5 % BSA and 5 % Goat serum in PBS) for 1 h. After that, sections were incubated with mouse anti-insulin (Proteintech Group, 66198-1-Ig, 1:100, Chicago, IL, USA) and rabbit anti-CD31 (Bioss, BS-0468R, 1:100, Beijing, China) overnight at 4 °C with the following primary antibodies diluted in blocking solution. Following decanting, the slides were washed with PBS (0.3 % Triton X-100) and incubated for 1 h at room temperature with fluorescein isothiocyanate (FITC)-conjugated Goat anti-Rabbit IgG (Invitrogen, F-2765, 2 µg/mL, Carlsbad, CA, USA) and Rhodamine Red-conjugated Goat anti-Mouse IgG (Jackson ImmunoResearch Laboratories, 115-295-144, 1:100, West Grove, PA, USA) in blocking solution. The slides were then washed with PBS and mounted with Vectashield antifade mounting medium containing DAPI (Vector Laboratories, Burlingame, CA, USA). Finally, the slides were visualized using confocal laser scanning microscope (CLSM).

## 2.23. Statistical analysis

All data were presented as mean ± SD. The statistical analysis was performed using GraphPad Prism (GraphPad Software, San Diego, CA, USA). To determine statistical significance, an unpaired Student's t-test was performed to compare two experimental groups, and ordinary one-way ANOVA was performed for the three experimental groups. Statistical significance was considered when the p-value was less than 0.05 or 0.01.

# 3. Results and discussion

## 3.1. Rapid Hislet formation using FS device

The overall process of forming Hislet is illustrated in Fig. 1A. After isolating 150 IEQ of pancreatic islets, they were dissociated into single cells and co-cultured with ADSCs in FS device. Given that 1 IEQ contains approximately 1500–2000 cells, we used  $2.5 \times 10^5$  ADSCs for co-culture to achieve 1:1 cell ratio [39]. To determine the shortest time required for spheroid formation, the cells were cultured in FS device for 1, 2, 4, 6, and 8 h. No spheroid formation was observed up to 6 h, however, after 8 h of culture, spheroids were successfully formed (Fig. 1B). We then compared spheroid formation under various conditions within the same culture period. Among different 3D culture methods, with or without ADSCs, and when co-culturing with pancreatic islet, only the acoustic pressure method with ADSCs resulted in loosely aggregated spheroids within 8 h (Fig. 1C). Notably, pancreatic islets did not float in the FS device, and ADSCs rarely attached to the surface of intact pancreatic islets. While non-adhesive U-shaped methods are established for 3D

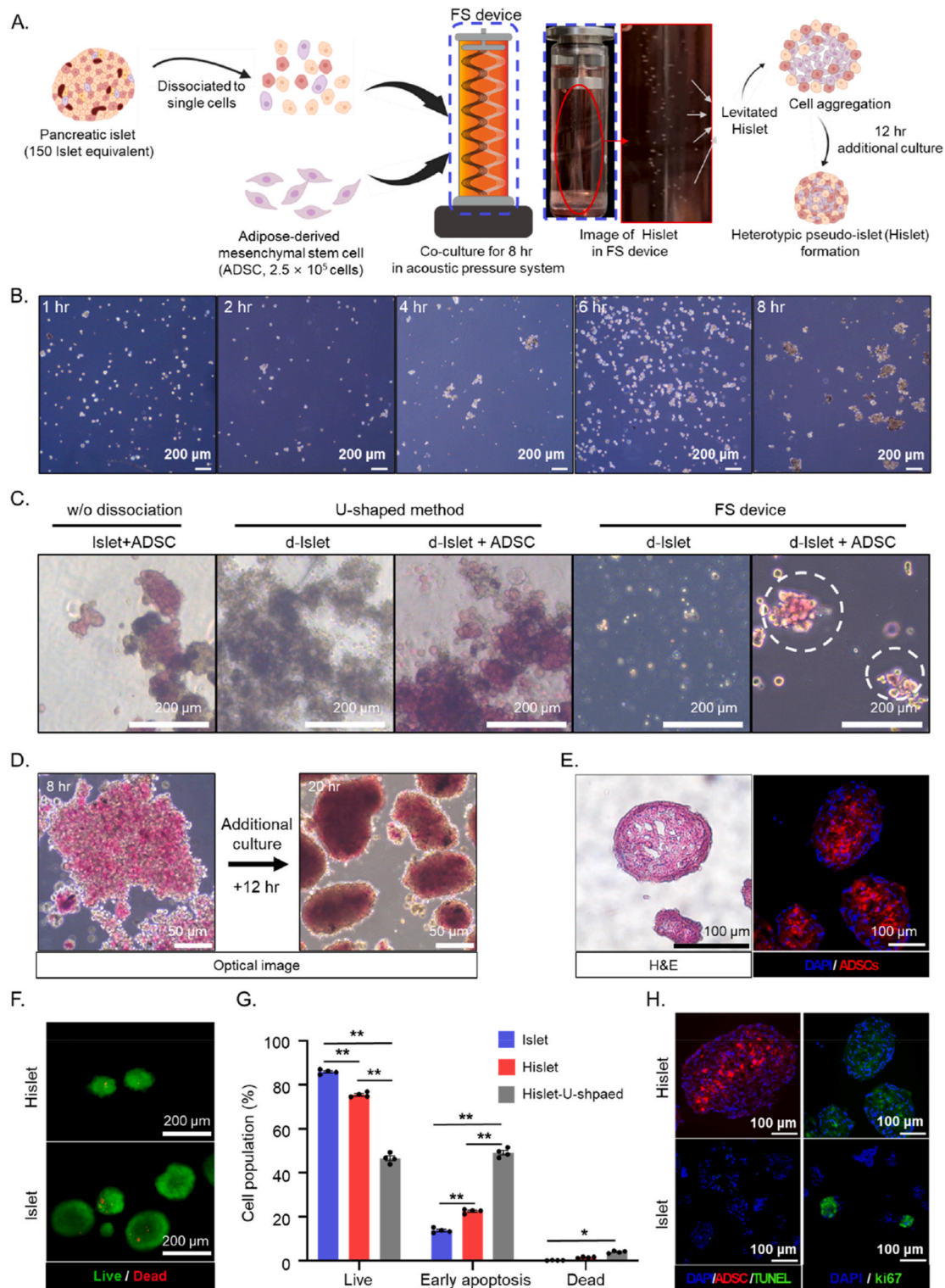


**Fig. 1.** Formation of heterotypic pseudo-islet (Hislet) based on a subaqueous free-standing 3D cell culture (FS) device. (A) Schematic figure showing the Hislet formation method. (B) Optical image of spheroid formation by using dissociated islet (d-islet) with adipose-derived mesenchymal stem cell (ADSC) in various time point (scale bar = 200  $\mu$ m). (C) Comparison of spheroid formation in conventional culture method (U-shaped well) and FS device with or without DiI-labeled ADSC (scale bar = 200  $\mu$ m). (D) Observation of spheroid compaction after additional culture of Hislet (scale bar = 50  $\mu$ m). (E) Hematoxylin & eosin staining image and fluorescent image of Hislet stained with DAPI (blue) and DiI-labeled ADSC (red, scale bar = 100  $\mu$ m). (F) Live (fluorescein diacetate (FDA), green) and dead (ethidium bromide (EB), red) assay results of islet and Hislet (Immediately after Hislet formation, scale bar = 200  $\mu$ m). (G) Cell viability analysis by staining annexin-V and 7-AAD with flow cytometry (FACS, n = 4). (H) Apoptotic activity evaluated with terminal deoxynucleotidyl transferase dUTP nick end labeling staining (TUNEL, green) for each group and immunofluorescence staining of ki67 (green) with DAPI (blue). Data are presented as the mean  $\pm$  SD, \* $p$  < 0.05, \*\* $p$  < 0.01 compared to each group.

spheroid culture, 8 h was insufficient for spheroid formation in both dissociated pancreatic islet cells (d-islet) and co-cultures of d-islet with ADSCs (Supplementary Fig. 1) [40]. The FS device-based d-islet culture showed more aggregation than the U-shaped method but remained less stable, and the spheroids were smaller compared to those formed with ADSCs co-culture.

Previous studies have shown that additional cultivation can induce spheroid compaction, enhancing cell-cell interactions and spheroid stability [41]. After 8 h culture in FS device, we compared additional cultures at time points of 0 h (immediately after removal from the FS device), 4 h, 8 h, and 12 h. Optical imaging revealed that spheroids without additional culture were loosely aggregated and exhibited brighter due to higher light transmittance. However, with increasing culture time, the spheroids became denser and darker in appearance. After an additional 12 h of culture in non-adhesive plate, the spheroids become more compact, as evidenced by decreased size and increased opacity (Fig. 1D and Supplementary Fig. 2A) [42]. Gene expression profiling demonstrated dynamic changes across key functional categories, providing insights into the Hislet maturation process. The expression levels of angiogenesis-related genes, including VEGF, ANGPT2, and FGF2, progressively increased over time, all peaking at 12 h. The ECM-related gene, fibronectin, also showed a significant increase at 12 h, suggesting that extended culture enhances spheroid stability by promoting ECM deposition necessary for structural integrity. The expression of INS1 and INS2, critical for insulin secretion, began increasing after 4 h and continued to rise through 12 h, indicating that functional maturation of insulin-producing cells initiates relatively early during the culture process. Likewise, expression of TGF- $\beta$ , an anti-inflammatory cytokine, started increasing at 8 h and peaked at 12 h, implying that immunomodulatory potential of the spheroids is enhanced as they stabilize over time (Supplementary Fig. 2B). These findings indicate that a 12 h additional culture period optimally enhances angiogenesis, ECM synthesis, insulin secretion, and anti-inflammatory cytokine production. H&E staining confirmed that extended culture increased protein expression on the outer layers of spheroids (Fig. 1E, left). Additionally, DiI-stained ADSCs revealed that ADSCs occupied the core of the compacted spheroids, while islet cells formed the outer layer (Fig. 1E, right). In an acoustic field, larger cells experience a stronger acoustic radiation force than smaller cells [43]. Since ADSCs are larger than dissociated islet cells, they are guided more rapidly to the pressure nodes created by the acoustic standing waves. This results in ADSCs aggregating at the core of the forming spheroid. Meanwhile, the smaller islet cells move more slowly and subsequently accumulate around the ADSCs, forming a shell-like structure. This phenomenon contributes to the rapid formation of Hislet with a core-shell architecture, where ADSCs occupy the center and islet cells form the outer layer, as observed in Fig. 1E.

Based on these findings, we established a protocol for Hislet formation: culturing cell in the FS device for 8 h followed by 12 h of subsequent culture. The resulting Hislet exhibited an average diameter of  $105.137 \pm 47.98 \mu\text{m}$  ( $n = 825$ , Supplementary Fig. 3), which is relatively smaller than that of conventional isolated pancreatic islets [14]. Live and dead assay revealed that Hislet exhibited similar viability to the Islet group (Fig. 1F). Flow cytometry with Annexin-5 and 7-AAD staining was performed to quantify the live cells in each group. The conventional Hislet formation method using a 5-day U-shaped culture (Hislet-U-shaped) showed significantly lower cell viability compared to the Islet group (Fig. 1G). TUNEL assay further demonstrated low levels of apoptosis in both Hislet and Islet groups, indicating comparable cell viability. Moreover, the cell proliferation marker Ki67 was observed in both groups (Fig. 1H). These results demonstrate that co-culturing with ADSCs in the FS device for 8 h, followed by an additional 12 h of culture, is sufficient for p-islet formation. Remarkably, only 20 h were required to form Hislet, a significant reduction compared to previous studies requiring at least 5 days for pseudo-islet formation [15–18].

The presence of ADSCs was crucial for rapid Hislet formation,

whereas without ADSCs, 8 h was insufficient for p-islet formation. ADSCs have a high ECM synthesis capacity, and ECM production supports the physical properties needed for spheroid formation [34,35]. Additionally, the effect of acoustic field on cell positioning enhances this process. The larger size of ADSCs allows them to aggregate more quickly at the pressure nodes, forming the spheroid core, while islet cells form the surrounding shell. Furthermore, previous we have study shown that acoustic stimulation in FS activates the PIEZO1/2 in ADSCs which has a crucial role in mechanobiological responses [44]. The activation of the PI3K pathway related to PIEZO1/2 activation was also enhanced and improved the ECM synthesis, which in turn contributes to a faster formation of spheroids [45,46]. Compared to Islet group, Hislet group showed significant increment of PIEZO1 and PIEZO2 gene (Supplementary Fig. 4). This characteristic enabled the formation of Hislet within a short time using the FS device. Additional culture time enhanced spheroid density and increased protein expression on the outer layers, which is beneficial for therapeutic applications due to increased stability [47].

To compare the effects of different cell ratios on Hislet formation, additional experiments were conducted using Islet-to-ADSC ratios of 3:1, 1:1, and 1:3, while maintaining the spheroid formation time at 8 h. After 8 h of culture, all groups exhibited spheroid formation to varying degrees; however, higher Islet ratios resulted in significantly smaller spheroids (Supplementary Fig. 5A, top and middle). To evaluate functionality, we analyzed insulin expression within the spheroids was analyzed. In the 3:1 group, no insulin-positive signals were detected, indicating that the small spheroids formed may consist primarily of ADSCs rather than functional islets (Supplementary Fig. 5A, bottom). In contrast, both the 1:1 and 1:3 groups exhibited insulin-positive signals, confirming that insulin-producing cells were involved in the spheroids (Supplementary Fig. 5A, bottom). Further functional assessment using GSIS assays showed that while insulin secretion increased slightly in the 1:3 group with higher glucose concentrations, its functionality was clearly inferior to that of the 1:1 group, which exhibited robust glucose-responsive insulin secretion (Supplementary Fig. 5B). These findings suggest that a higher Islet ratio (e.g., 3:1) requires prolonged culture times to form functional spheroids, undermining the advantage of rapid aggregation offered by the FS device. On the other hand, a higher ADSC ratio (e.g., 1:3) forms spheroids quickly but results in reduced glucose-dependent insulin secretion, making it less effective for Type 1 diabetes treatment. Ultimately, the 1:1 ratio offers the optimal balance between rapid Hislet formation and robust functional performance, supporting its use as a promising therapeutic platform.

Isolated islets often have diameters exceeding 200  $\mu\text{m}$ , leading to low cell viability after engraftment and difficulty in nutrient delivery to the core of islet [14,48]. The Hislet averaged 105  $\mu\text{m}$  in diameter, notably smaller than isolated pancreatic islets, which may enhance survival and glucose-responsive insulin secretion [6,19,49]. While p-islet formation allows for controlled, smaller size, traditional methods face disadvantage such as cell loss due to long-term culture. Our method of co-culturing with ADSCs in the FS device enabled Hislet formation within a day, significantly improving cell viability compared to conventional methods, with similar cell viability of Islet. Additionally, Ki67 expression in Hislet correlated positively with key markers for insulin secretion, and co-culturing with ADSCs has been shown to increase Ki67 expression in islet cells [50]. These findings confirm that FS device-based Hislet formation is efficient and maintains high cell viability.

### 3.2. Enhanced ECM expression, cell-cell connection, angiogenesis, and immunomodulation effect in Hislet

Next, we investigated the ECM expression and cell-cell adhesion molecules to assess the structural and functional integrity of Hislet. Collagen 1 (Col1) and laminin are major ECM components, while Connexin 43 (Con43) and E-cadherin (E-cad) are representative cell-cell



connection markers [51–53]. Immunofluorescence staining demonstrated that both groups expressed Col1, Laminin, Con43, and E-cad; however, the Hislet group exhibited higher fluorescence intensity, indicating elevated expression compared to Islet group (Fig. 2A). Western blot analysis showed that laminin and Con43 expression were significantly higher in Hislet group, with laminin expression being

approximately 3-fold higher and Con43 approximately 2-fold higher than in the Islet group (Fig. 2B). Additionally, integrin- $\alpha_v$ , a protein mediating cell-ECM interactions, was significantly upregulated in Hislet group (Fig. 2B) [54].

These results suggest that Hislet had enhanced structural integrity due to increased ECM production and cell-cell adhesion. The

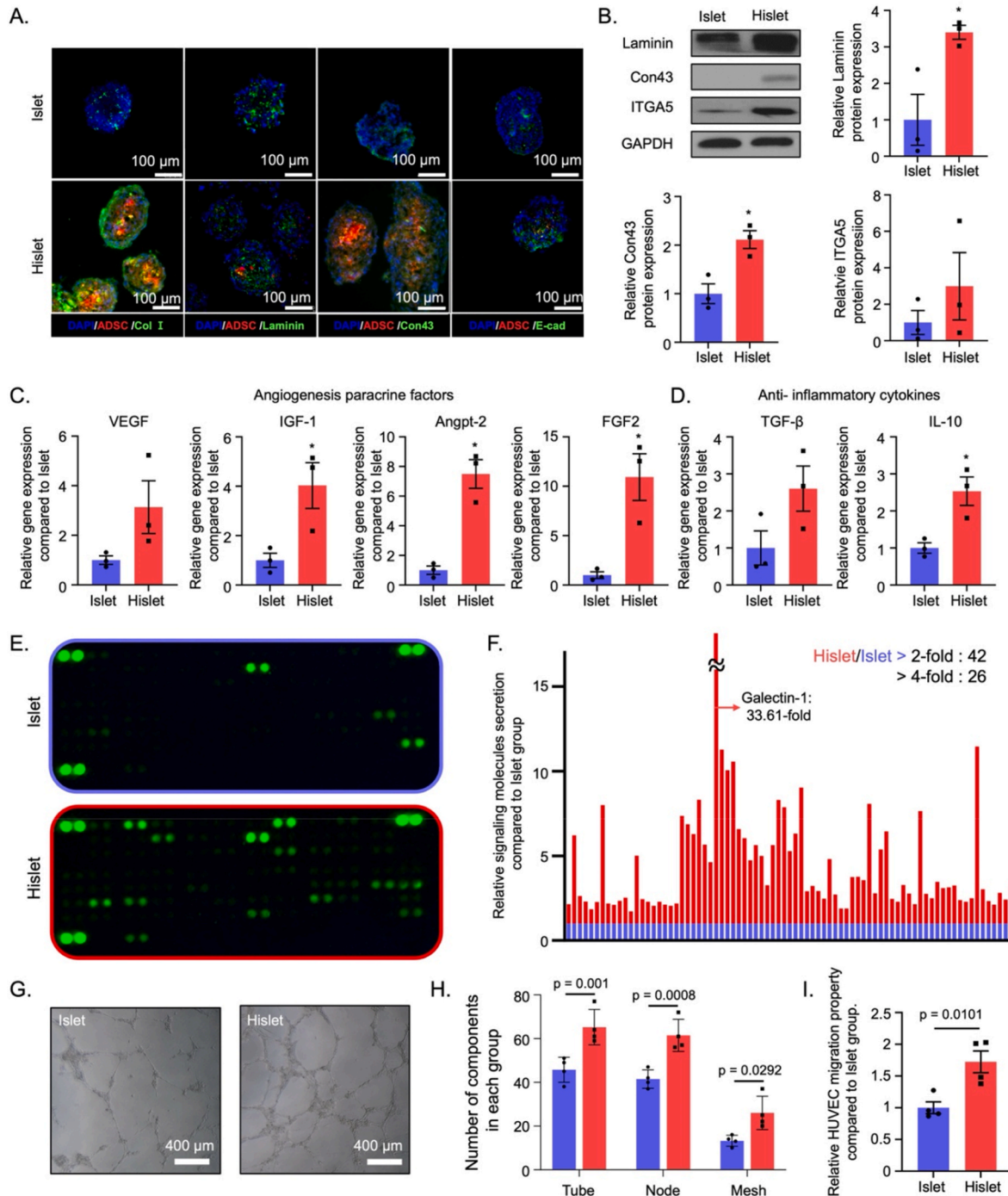


**Fig. 2.** Evaluation of gene and protein expression related to extracellular matrix (ECM), cell-cell, cell-ECM connection, various secretion factors, and angiogenesis. (A) Fluorescence images of Islet and Hislet stained with collagen 1 (Col 1), laminin, connexin 43 (Con43), and E-cadherin (E-cad) (green). DAPI (blue) was stained for nucleus in entire cells and DiI (red) used for labeling the ADSC (scale bar = 100  $\mu$ m). (B) Comparison of protein expression in each group as evaluated by Western blot analysis ( $n = 3$ ,  $*P < 0.05$  compared to Islet). Relative (C) angiogenesis and (D) anti-inflammatory cytokine gene expression compared to Islet group evaluated by real-time quantitative reverse transcription polymerase chain reaction (qRT-PCR,  $n = 3$ ,  $*P < 0.05$  compared to Islet). (E) Images of cytokine array result of collected conditioned media (CM) collected from each group and (F) quantification of the cytokine array. (G) Image of tube formation assay after treating CM from each group to human umbilical vein endothelial cells (HUVEC, 6 h treatment,  $n = 4$  scale bar = 400  $\mu$ m). (H) Quantification of tube, node, mesh after HUVEC tube formation in each group ( $n = 4$ ). (I) Quantification of closed area of HUVEC after migration ( $n = 4$ ). Data are presented as the mean  $\pm$  SD.



upregulation of ECM components like laminin and Col1 provides a supportive microenvironment that can improve cell viability and function. Elevated levels of cell adhesion molecules such as Con43 and E-cad facilitate better cell-cell communication, which is crucial for synchronized insulin secretion and overall islet function [55,56]. The increase in ECM expression and cell-cell connections supports stable glucose-responsive insulin secretion and enhances cell viability, as well as the structural integrity of the Hislet.

We then examined the angiogenic and immunomodulatory properties of Hislet. Angiogenesis-related genes such as *VEGF*, *IGF-1*, *Angpt-2*, and *FGF2* were significantly upregulated in the Hislet group, with fold increases ranging from 2- to 4-fold compared to the Islet group (Fig. 2C). Anti-inflammatory cytokines including *IL-10* and *TGF- $\beta$*  were also significantly upregulated in Hislet group (Fig. 2D). These gene expression results suggest that Hislet had a higher potential to promote angiogenesis and exhibit immunomodulatory effect. To assess the actual secretion of angiogenesis- and immunomodulation-related cytokines, chemokines, and growth factors, we performed a cytokine protein array using CM collected from each group. The Hislet group displayed more positive signals compared to the Islet group (Fig. 2E). Protein array revealed that out of 79 proteins analyzed, 42 were secreted at levels at least 2-fold higher in the Hislet group, and among these, 26 proteins were secreted at levels 4-fold higher (Fig. 2F). Key factors significantly increased in the Hislet group included VEGF, IGF-1, Angpt-2, FGF2, IL-10, and TGF- $\beta$ . A full list of the paracrine factors and their fold changes (Hislet/Islet) is provided in Supplementary Table 1. The upregulation of angiogenic factors promote endothelial cell migration and vascular stabilization, crucial for nutrient and oxygen supply to transplanted islets [57–61]. Furthermore, CM from the Hislet group induced significantly more tube formation of HUVECs compared to CM from the Islet group (Fig. 2G). Quantification of the number of tubes, nodes, and meshes, tube formation parameters, are 1.42-fold, 1.48-fold and 1.96-fold higher, respectively, in the Hislet group, indicating a stronger angiogenic effect of Hislet (Fig. 2H). Gene expression profiling further demonstrated significant upregulation of angiogenesis-related genes such as VEGF and ANGPT2 in the Hislet group, whereas CXCR4 expression showed a slight, but statistically non-significant, increase (Supplementary Fig. 6). These results suggest that Hislet enhance endothelial sprouting and migration, crucial for new blood vessel formation. Additionally, treatment with CM derived from Hislet induced a strong migratory response in HUVEC (Fig. 2I, Supplementary Fig. 7).

Pancreatic islets secrete a diverse array of proteins, including insulin, glucagon, somatostatin, ghrelin, and pancreatic polypeptide [62]. However, they exhibit a relative deficiency in their capacity to secrete angiogenic factors necessary for post-transplantation vascularization and immunomodulatory cytokines that could mitigate immune responses [63,64]. In contrast, ADSCs are known to possess robust angiogenic and immunomodulatory capabilities, attributed to their diverse secretion of growth factors and cytokines [65]. By incorporating ADSCs into the formation Hislet, we have conferred intrinsic angiogenic and immunomodulatory properties to the Hislet themselves. Angiogenesis following transplantation is critical for the survival of transplanted cells [66]. The enhanced tube formation and migratory capacity of HUVECs observed *in vitro* suggest that Hislet possess greater neo-vascularization potential post-transplantation, thereby improving graft survival. This approach leverages the paracrine effects derived from ADSCs to enhance the therapeutic potential of islet transplantation.

Overall, these results demonstrate that Hislet exhibit enhanced secretion of angiogenic and immunomodulatory cytokines, contributing to improved islet survival and function. The multifunctional properties of Hislet, including their ability to promote vascularization and modulate immune responses, suggest that they have significant potential for improving the outcomes of islet transplantation.

### 3.3. Comparative RNA-sequencing analysis of Hislet and Islet

To elucidate the molecular mechanisms underlying the enhanced functionality of Hislet over conventional Islet, we conducted comprehensive RNA sequencing followed by transcriptomic analyses. A Venn diagram revealed that while a substantial portion of genes (92 %, 17,706 genes) are shared between Hislet and Islet, there are distinct gene sets unique to each: 643 genes are unique to Hislet, and 858 genes are unique to Islet (Fig. 3A). This significant overlap reflects their common cellular origin; however, the unique gene expression profiles suggest functional divergences arising from the co-culture with ADSCs and the use of the FS device in Hislet formation. PCA demonstrated a clear separation between Hislet and islet samples, with the first principal component (PC1) accounting for 67.3 % of the variance (Fig. 3B). This indicates distinct global gene expression patterns between the two groups, likely associated with the unique structural characteristics and functional enhancements of Hislet. Hierarchical clustering of differentially expressed genes (DEGs) further emphasized these differences (Fig. 3C). Notably, genes associated with ECM components and cell–cell adhesion molecules were upregulated in Hislet. For example, the expression levels of *Col1*, *laminin*, *Con43*, and *E-cad* were significantly higher in Hislet compared to Islet. These findings are consistent with our earlier immunofluorescence and Western blot analyses (Fig. 2A and B), suggesting that Hislet had enhanced structural integrity and cell-cell communication, which may contribute to their improved viability and insulin secretion.

Genes related to angiogenesis were also significantly upregulated in Hislet. Key pro-angiogenic factors such as *VEGFA*, *ANGPT1*, and *FGF2* showed increased expression (Fig. 3D). This upregulation indicates a heightened capacity for promoting vascularization, which is crucial for nutrient delivery and graft survival post-transplantation. Genes involved in immune regulation exhibited differential expression as well. Anti-inflammatory cytokines including *IL-10*, *TGF- $\beta$* , and *IL-4* were upregulated, whereas pro-inflammatory markers like *IL-1* and *TNF- $\alpha$*  were downregulated in Hislet (Fig. 3E). These changes suggest an enhanced immunosuppressive environment in Hislet, which could contribute to improved graft survival by mitigating immune rejection. Importantly, genes critical for insulin production and secretion, such as *INS1* and *PDX1*, were more highly expressed in Hislet compared to Islet (Fig. 3F). This elevated expression indicates that Hislet may have improved glucose-responsive insulin secretion capabilities. The smaller size and increased cell-cell interactions of Hislet, resulting from the FS device-assisted formation and ADSC co-culture, likely contribute to this functional enhancement.

Gene Ontology (GO) enrichment analysis highlighted several biological processes that are enriched in Hislet, including tube morphogenesis, ECM organization, immune regulation, and cell proliferation (Fig. 3G). These pathways corroborate our experimental observations of enhanced structural stability, angiogenesis, immunomodulation, and cell viability in Hislet. Supplementary volcano plots provided additional insights into specific gene sets associated with processes such as cell morphogenesis, tissue development, and skeletal system organization, further emphasizing the broad functional capabilities of Hislet compared to conventional Islet (Supplementary Fig. 8).

In summary, the transcriptomic analyses reveal that Hislet possess a distinct and optimized gene expression profile characterized by upregulation of genes involved in ECM composition, angiogenesis, immune modulation, and insulin secretion. These molecular features align with the functional enhancements demonstrated in earlier sections and suggest that Hislet is better equipped for therapeutic applications. These findings also set the stage for further investigation into the glucose-responsive insulin secretion capabilities of Hislet, which will be discussed in the following section. Understanding how these molecular and functional improvements translate into enhanced insulin secretion is crucial for evaluating the potential of Hislet in treating diabetes through islet transplantation.

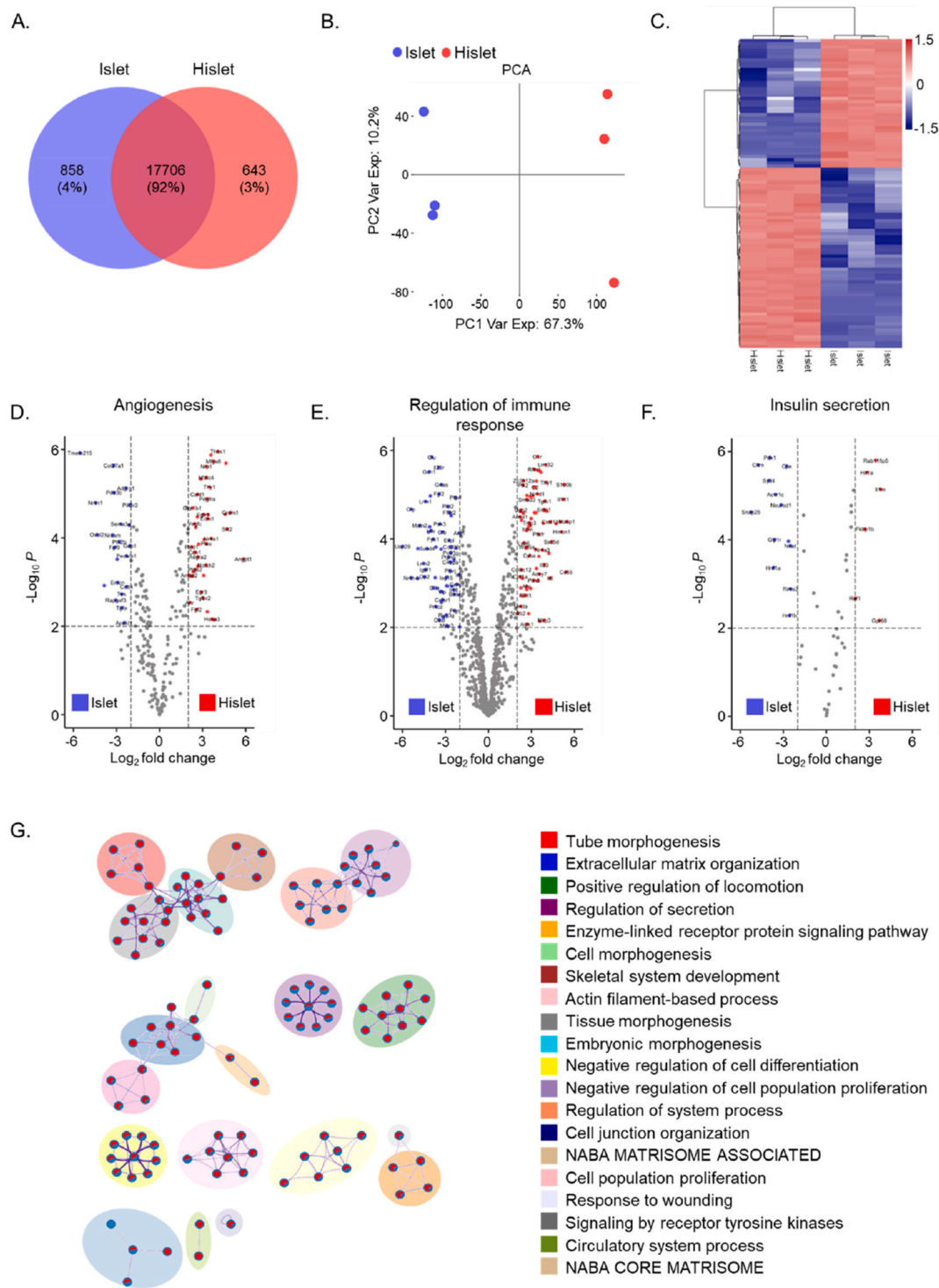


**Fig. 3.** RNA-sequencing result of comparing Islet and Hislet group. (A) Venn diagram showing the overlap and unique genes between Islet and Hislet groups, with 17,706 shared genes, 858 islet-specific genes, and 643 Hislet-specific genes. (B) PCA plot demonstrating the separation between Hislet and Islet samples. PC1 explains 67.3 % of the variance, indicating distinct expression profiles between the groups. (C) Heatmap of differentially expressed genes, with clustering showing distinct upregulation patterns in Hislet relative to Islet. (D–F) Volcano plot of genes associated with (D) angiogenesis, (E) immune-regulation, and (F) insulin secretion. (G) GO enrichment network map showing the biological processes enriched in Hislet.

**3.4. Verifying the glucose-responsive insulin secretion and long-term survival**

In the next step, we investigated the insulin secretion properties of Hislet in response to varying glucose concentrations. Insulin secretion-related gene expressions revealed increased PDX1 and GLUT1

expressions in the Hislet group compared to the Islet group, while HK1 levels remained similar and UCP2 expression was decreased (Fig. 4A). The elevated PDX1 suggests enhanced  $\beta$ -cell function and survival, as this gene plays a crucial role in insulin production and  $\beta$ -cell maintenance [67]. Increased GLUT1 expression indicates improved glucose uptake, especially under hypoxic conditions [68], while decreased

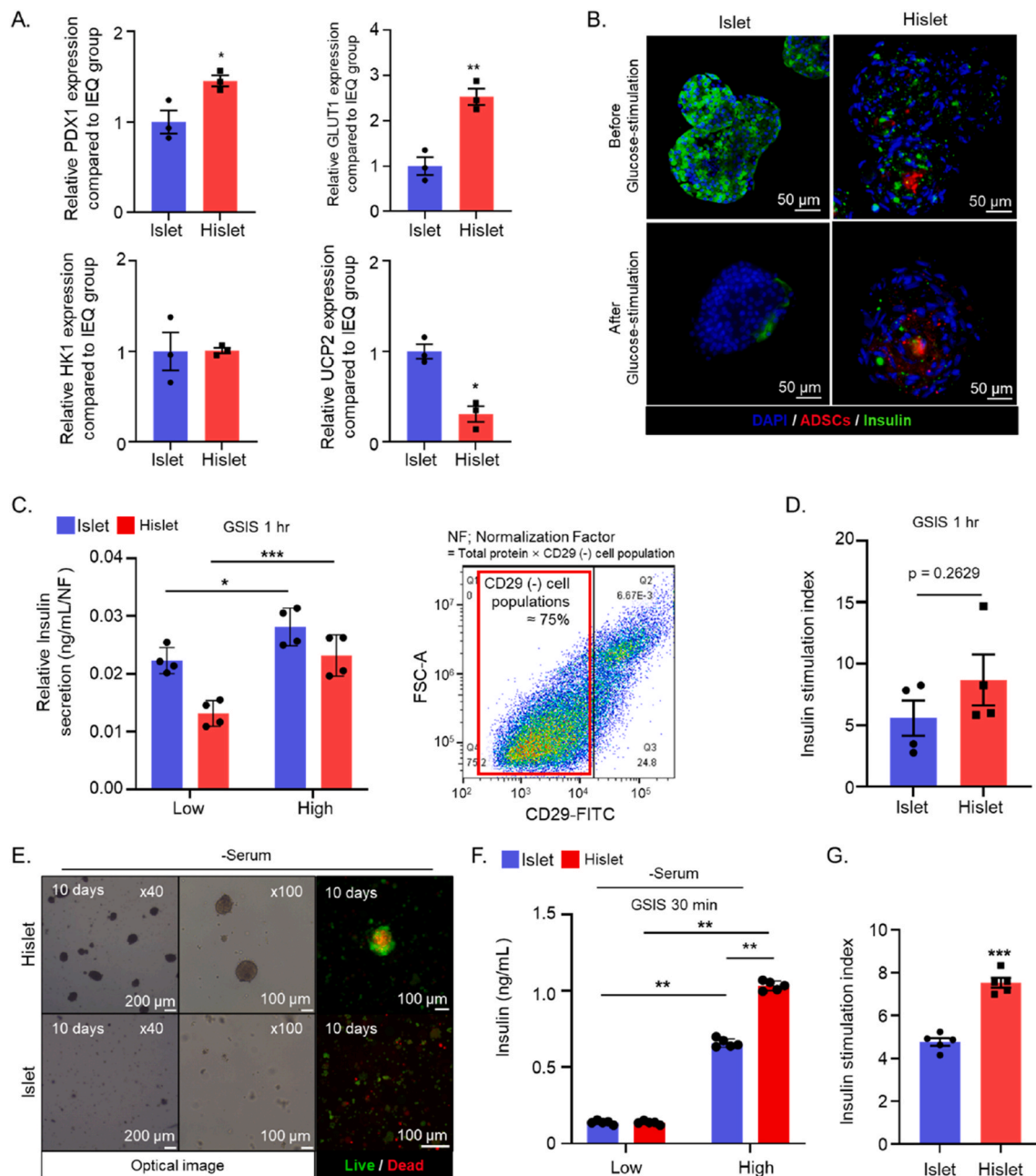


**Fig. 4.** Validation of glucose-responsive insulin secretion property and enhanced long-term survival. (A) Result of insulin secretion and glucose transporter related gene expression in each group as evaluated by qRT-PCR ( $n = 3$ ,  $*P < 0.05$ ,  $**P < 0.01$  compared to Islet group) (B) Fluorescence image of each group with immunofluorescence insulin staining (green, scale bar = 50  $\mu$ m). (C) Glucose-stimulated insulin secretion (GSIS) assay of each group according to the low (2.8 mM) and high (20.2 mM) glucose concentration for 1 h as evaluated by enzyme-linked immunosorbent assay (ELISA) normalized with protein contents and ratio of CD29 negative cells as evaluated by FACS ( $n = 4$ ,  $*P < 0.05$ ,  $***P < 0.001$  compared to each group). (D) Insulin stimulation index of each group calculated by insulin secretion amount at high glucose divided by insulin secretion amount at low glucose ( $n = 4$ ), (E) Optical and fluorescence image of live and dead assay images after in the serum-free media culture for 10 days (scale bar = 200  $\mu$ m for leftmost panel, 100  $\mu$ m for others). (F) GSIS assay of each group after culturing in serum-free media for 10 days ( $n = 5$ ,  $*P < 0.05$ ,  $**P < 0.001$  compared to each group). (G) Insulin stimulation index of each group ( $n = 5$ ,  $***P < 0.001$  compared to Islet group.) Data are presented as the mean  $\pm$  SD.

UCP2, a negative regulator of insulin secretion, may enhance glucose-stimulated insulin secretion [69,70]. Hislet secreted IGF-1 2-fold higher than Islet (Fig. 2E–Supplementary Table 1), and IGF-1 could induce the increment of the PDX1 gene expression in Hislet [67]. These gene expression patterns suggest that Hislet may have advantages in glucose uptake and insulin secretion compared to Islet.

We assessed glucose-stimulated insulin secretion (GSIS) using low-glucose (2.8 mM) and high-glucose (20.2 mM) solutions. Immunofluorescence staining showed that both Islet and Hislet groups contained

insulin prior to glucose stimulation and secreted insulin after glucose stimulation for 30 min (Fig. 4B). The GSIS assay, normalized to total protein content and the proportion of CD29-negative cells [71], demonstrated that both groups increased insulin secretion with higher glucose concentrations (Fig. 4C). The insulin stimulation index was slightly higher in the Hislet group compared to the Islet group, although the difference was not statistically significant (Fig. 4D), indicating comparable glucose responsiveness between the groups. To simulate post-transplantation conditions where nutrient supply is limited, we

cultured both groups in serum-free media for 10 days. After this period, Hislet maintained their spheroid structure, while the Islet group showed dissociation and cell debris (Fig. 4E). Live/dead staining revealed viable cells in both groups, but Islet cells were primarily single cells. To mimic the hypoxic conditions encountered after transplantation, Islet and Hislet were cultured under 5 % O<sub>2</sub>, a level lower than the physiological oxygen concentration of healthy kidney [72]. Under these conditions, Hislet not only maintained their spheroid structure more effectively than Islet but also exhibited fewer dead cells (Supplementary Fig. 9). Post-culture GSIS assays indicated that both groups still responded to glucose, but the insulin stimulation index was significantly higher in the Hislet group (Fig. 4F and G). This suggests that Hislet has superior long-term survival and insulin secretion function under harsh conditions even without segregation of ADSCs and islet cells. Immediately after

transplantation, islets lack direct vascular connection, creating harsh conditions where transplanted cells struggle to receive sufficient nutrients [73]. Islet must survive without sufficient nutrient supply until new blood vessels form, typically 7–14 days after transplantation [74]. To simulate this condition, we conducted experiments under serum-free conditions, where essential nutrients for cell survival were absent. The long-term culture suggested that Hislet has a higher potential for survival after transplantation and a higher insulin stimulation index, likely due to better-preserved functionality from increased cell viability. While increased PDX1 expression has been associated with enhanced beta-cell survival and function, the precise mechanisms underlying the maintenance of structure, survival, and function in Hislet during long-term culture remain to be fully elucidated [75]. It is hypothesized that the capacity of stem cells to synthesize hypoxia-inducible factors (HIFs)

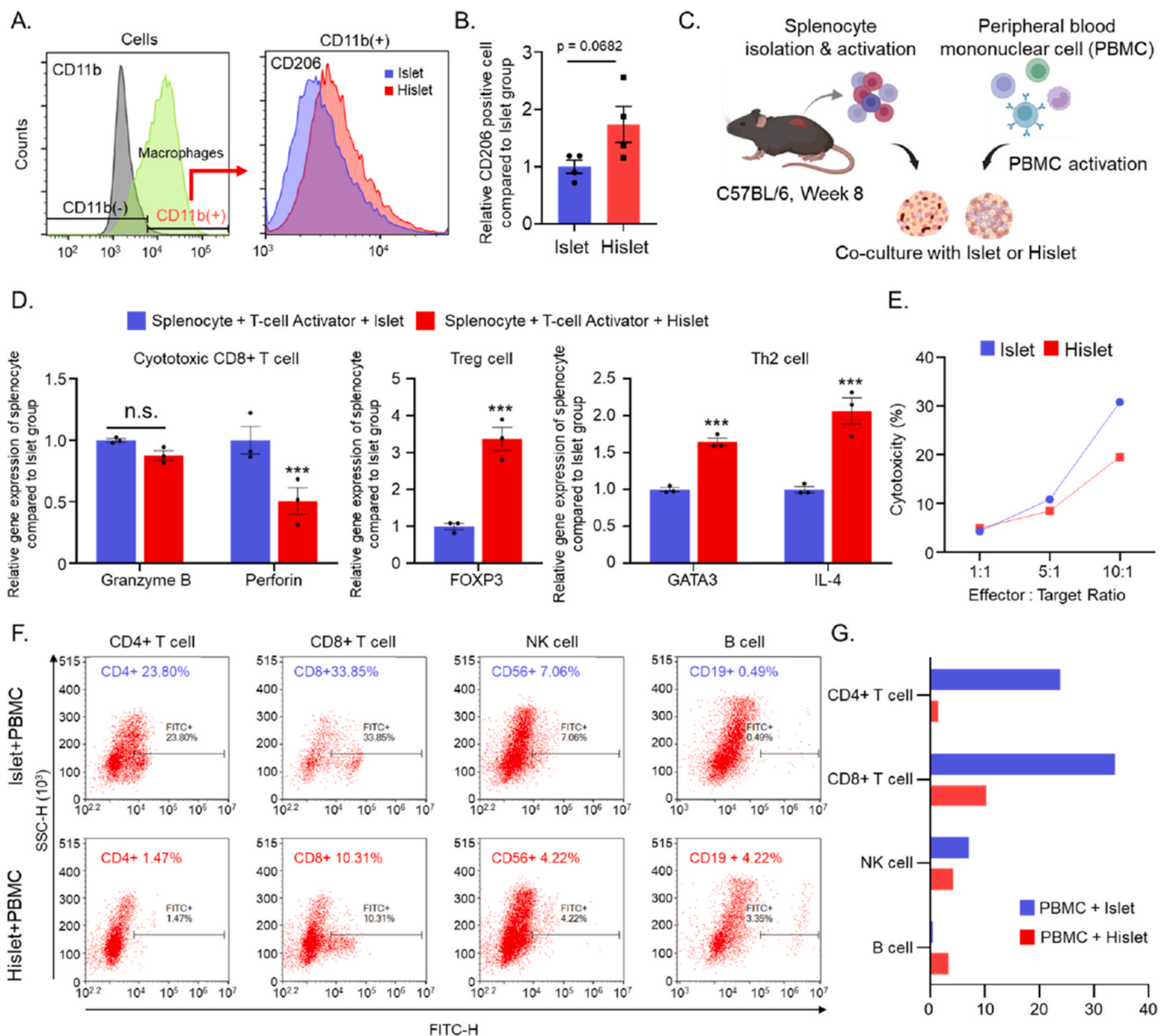


**Fig. 5.** Evaluation of immunomodulation effect of Hislet. (A) Result of M1-M2 transition assay after treating CM from each group analyzed with FACS and (B) quantification of CD206 positive cells ( $n = 4$ ). (C) Schematic figure of *in vitro* immunomodulation assay with splenocyte and peripheral blood mononuclear cell (PBMC) (D) Cytotoxic CD8<sup>+</sup> T cell, Treg cell, and Th2 cell related gene expression of splenocyte after co-cultured with T-cell activator and Islet or Hislet ( $n = 3$ , \*\*\* $P < 0.001$  compared to Islet group). (E) Evaluation of immune cell-mediated cytotoxicity of Islet and Hislet after co-cultured with activated PBMC assessed with lactate dehydrogenase assay (Effector: activated PBMC, Target: Islet or Hislet). (F) FACS result stained with CD4 (CD4<sup>+</sup> T cell), CD8 (CD8<sup>+</sup> T cell), CD56 (NK cell), and CD19 (B cell). (G) Comparison of each immune cell population between Islet and Hislet group. Data are presented as the mean  $\pm$  SD.



under adverse conditions, coupled with the upregulation of PDX1 expression, contributes to the inhibition of apoptosis in these cellular aggregates [76]. This interplay between HIFs and PDX1 may represent a key adaptive response that promotes islet resilience in extended culture conditions, though further research is needed to delineate the specific pathways involved in this process. Altogether, Hislet retain their primary function of glucose-responsive insulin secretion for controlling glucose levels even after long-term culture under conditions that mimic transplantation.

### 3.5. Enhanced Immunomodulation effect in Hislet

In the next step, we evaluated the immunomodulatory properties of Islet and Hislet, which play a crucial role in graft survival following transplantation due to immune response at the transplantation site. Transplanted islets are often attacked by the host's immune cells, leading to inflammatory responses that can decrease islet survival [77]. Preventing immune reaction is therefore a key strategy for enhancing graft survival. To assess immunological interactions, we utilized various types of immune cells, including macrophages, splenocytes, and PBMCs. First, we tested M1-M2 transition effect by treatment with Islet and Hislet CM to M1 macrophage. Hislet CM treated M1 macrophage showed increment of M2 macrophages transition, with a 1.7-fold increase compared to the Islet group (Fig. 5A and B). Macrophages, an innate immune cells, play a pivotal role in determining the initiation of adaptive immunity in response to transplanted cells [78]. Macrophages have a two phenotypes: pro-inflammatory M1 macrophages and anti-inflammatory M2 macrophages [79]. While M1 macrophages are essential during the initial inflammatory response post transplantation [80], prolonged M1 activity can damage transplanted cells and surrounding tissues, leading to graft rejection [81]. Therefore, promoting the transition from M1 to M2 macrophages after the initial inflammation is crucial for the survival of the transplanted islets [82]. Inducing M1-to-M2 transition has been reported to improve the viability of grafted islets [83]. This demonstrates a substantial M1-to-M2 transition, suggesting enhanced immunomodulatory potential of Hislet. To more accurately evaluate the immunomodulatory effects of Hislet, we assessed their immunosuppressive capacity by directly co-culturing activated splenocytes and PBMCs with both Islet and Hislet (Fig. 5C). These immune cell populations contain T cells, B cells, NK cells, and macrophages, all of which are involved in graft rejection. Gene expression profiling of splenocytes following co-culture revealed notable differences. While there was no significant difference in the expression of Granzyme B, a cytotoxic protein used by CD8<sup>+</sup> T cells to kill target cells, the expression of Perforin, another key cytotoxic molecule, was reduced by approximately 50 % in the Hislet group compared to the Islet group (Fig. 5D–Cytotoxic CD8<sup>+</sup> T cell) [84]. The results suggests that Hislet may attenuate CD8<sup>+</sup> T cell-mediated cytotoxicity by specifically downregulating Perforin production. Additionally, FOXP3 expression, a marker of regulatory T cells (Tregs), was increased in the Hislet group indicating enhanced Treg activation (Fig. 5D–Tregs). Tregs are known to suppress immune responses effectively and reduce graft rejection through mechanisms such as cytokine secretion (e.g., IL-10, TGF- $\beta$ ) and inhibition of effector T cell activity [85]. These findings indicated that Hislet is not suppress cytotoxic immune responses but also promote immune tolerance through Treg activation. In the context of transplantation, shifting the immune balance from Th1 to Th2 dominance is crucial for reducing rejection [86]. In our co-culture system, Hislet treatment resulted in increased expression of GATA3, a key transcription factor for Th2 differentiation, as well as upregulation of IL-4, a cytokine secreted by Th2 cells that suppresses immune responses (Fig. 5D–Th2 cell) [87,88]. Conversely, a pro-inflammatory cytokine IFN- $\gamma$  secreted by Th1 cells, showed a slight but non-significant decrease in the Hislet group, while the expression of T-bet, a master regulator of Th1 differentiation, remained unchanged (Supplementary Fig. 10) [87]. These results suggested that Hislet may

shift the Th1/Th2 balance toward a Th2-dominant profile, thereby enhancing immune tolerance without significantly altering Th1-specific factors.

To further assess immune modulation, we performed additional co-culture experiments to assess the interactions between activated PBMCs and Islet or Hislet. Islets or Hislet were co-cultured with increasing numbers of PBMCs to analyze cytotoxicity and alterations in immune cell populations, specifically CD4<sup>+</sup> T cells, CD8<sup>+</sup> T cells, NK cells, and B cells. The results demonstrated that Hislet significantly better survival than Islet under increasing effector-to-target ratios indicating superior resistance to immune-mediated cytotoxicity (Fig. 5E). This indicates that Hislet possess enhanced capabilities for modulating cytotoxic immune cells, including NK cells and cytotoxic T cells, which directly mediate cell death. Flow cytometry analysis revealed that the proportions of CD4<sup>+</sup> T cells, CD8<sup>+</sup> T cells, and NK cells—key mediators of graft rejection—were significantly reduced in the Hislet group, compared to the Islet group (Fig. 5F and G) [89]. In contrast, the population of B cells increased in the Hislet group (Fig. 5F and G). The B cell population increased in the Hislet group. While B cells have dual roles in graft rejection depending on their subtypes, the observed decrease in cytotoxicity in the Hislet group suggests that the increased B cell population likely promotes immune tolerance [90]. Overall, these findings highlight that Hislet modulates immune responses through multifaceted mechanisms, including the secretion of ADSC-derived factors, the facilitation of the transition from pro-inflammatory M1 macrophages to anti-inflammatory M2 macrophages, and suppression of differentiation and activity of immune cells responsible for graft rejection (CD4<sup>+</sup> T cells, CD8<sup>+</sup> T cells, and NK cells) and enhance regulatory and Th2-associated immune profiles. These effects collectively result in lower cytotoxicity and improved immune compatibility in the context of islet transplantation.

Taken together, our results highlight the potent immunomodulatory properties of Hislet and their potential to reduce graft rejection. These features make Hislet a promising therapeutic strategy for improving graft survival and reducing immune-mediated damage in Type 1 diabetes treatment.

### 3.6. Evaluation of *in vivo* functionality of Hislet transplantation

To further evaluate the long-term glucose-regulating capacity and therapeutic potential of Hislet for T1DM, *in vivo* transplantation studies were conducted. After Specifically, Hislets (Equivalent to 400 IEQ) were transplanted under the kidney capsule of BALB/c nude mice (Fig. 6A). Non-fasting blood glucose (NBG) levels were monitored for 21 days post-transplantation. Islets were used as a control group, while the experimental group received Hislets. Both the islet and Hislet groups successfully maintained normoglycemic levels throughout the observation period (Fig. 6B), indicating that Hislet retained functional glucose-regulatory ability *in vivo*, comparable to that of Islet. To confirm that glycemic control was mediated by the transplanted grafts rather than endogenous insulin recovery, the grafts were surgically removed on day 21. Following graft removal, both groups exhibited a rapid return to hyperglycemia, demonstrating that blood glucose regulation was directly attributable to the transplanted grafts (Fig. 6B, Day 21). To further assess the glucose responsiveness of the grafts under physiological conditions, an intraperitoneal glucose tolerance test (IPGTT) was performed on day 20 post-transplantation. Hislet-transplanted mice exhibited a less maximum blood glucose level during IPGTT and lower area under the curve (AUC) compared to mice transplanted with naïve islet (Fig. 6C–D) supporting the notion that Hislet exhibit enhanced glucose responsiveness and insulin secretion capacity. Immunofluorescence staining of graft-bearing kidneys harvested on day 21 revealed comparable insulin-positive cell masses in both groups (Fig. 6E). However, CD31 expression, a marker for vascular endothelial cells [91] was more prominently observed in the Hislet group, suggesting enhanced angiogenesis at the graft site.

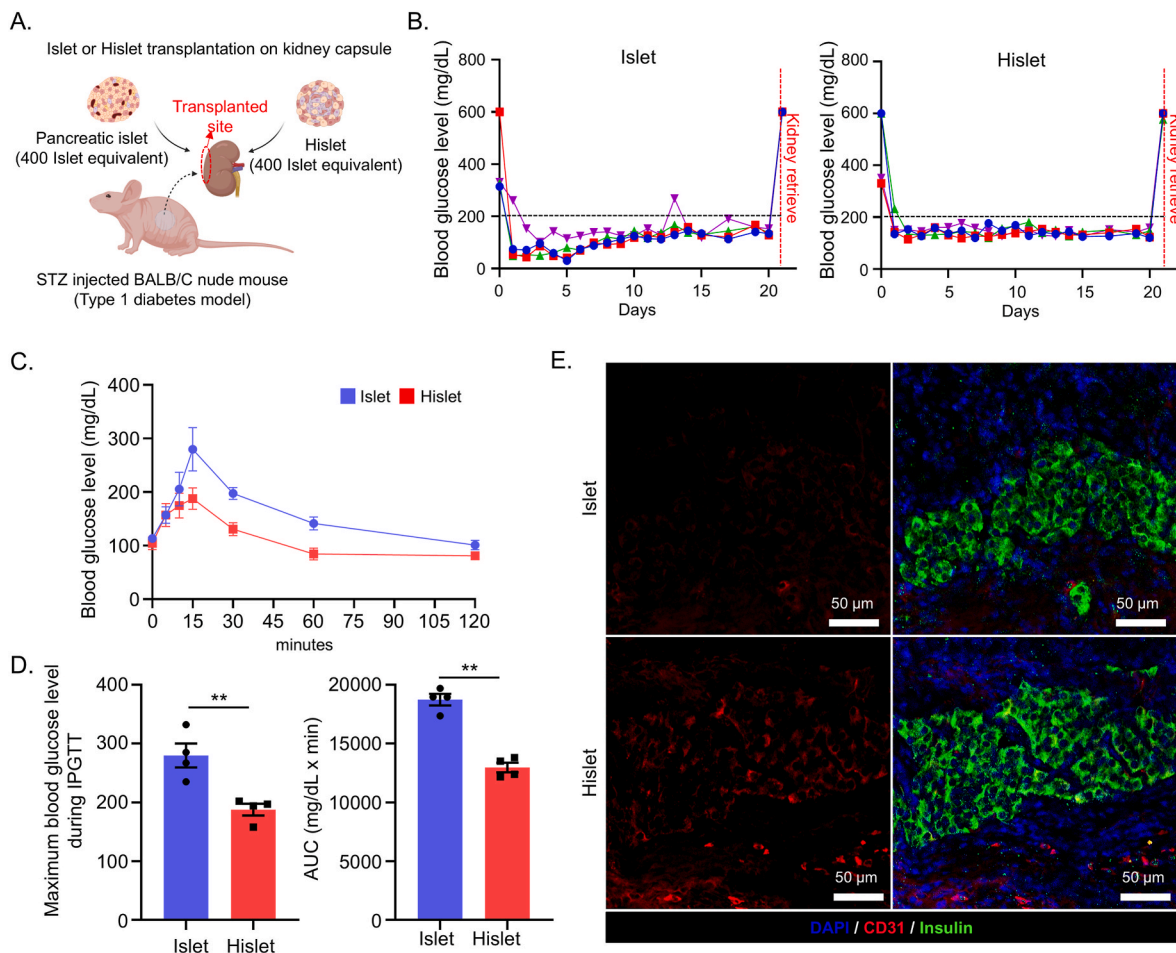


**Fig. 6.** Therapeutic effect validation of Hislet for *in vivo* type 1 diabetes (T1DM) model functionality and immunofluorescence imaging of Hislet (A) Schematic figure showing islet transplantation under kidney capsule for *in vivo* T1DM model (B) Non-fasting blood glucose levels of T1DM mice transplanted with 400 IEQ Islet (n = 4) and 400 IEQ equivalent Hislet (n = 4). (C) Intraperitoneal glucose tolerance test (IPGTT) of Islet (n = 4), Hislet (n = 4) on day 20 post-transplantation. (D) Maximum blood glucose level and area under the curve of IPGTT (n = 4) (E) Immunofluorescence staining of kidney retrieved from Islet and Hislet group stained with insulin (Green) and CD31 (Red) on day 21 after transplantation. (scale bar = 50  $\mu$ m). Data are presented as the mean  $\pm$  SD, \*\*p < 0.01 compared to each group.

A comprehensive analysis of the *in vivo* data revealed that while both groups effectively maintained normoglycemia, the Hislet group demonstrated superior functional performance as evidenced by the lower AUC during IPGTT. This suggests that Hislet respond more sensitively to changes in glucose concentration, releasing insulin in a glucose-dependent manner. A lower AUC further indicates a stronger functional integration between insulin-secreting cells and host vasculature [92]. Additionally, the increased CD31 expression observed in the Hislet group supports the conclusion that Hislet promote vascular formation *in vivo*, potentially contributing to improved graft survival and long-term function [93]. These findings indicate that the angiogenic properties of Hislet observed *in vitro* are recapitulated *in vivo*, reinforcing their potential utility. Collectively, Hislet generated via FS device-based co-culture with ADSCs exhibit robust *in vivo* functionality, enhanced vascularization, and superior glucose responsiveness, making them a promising therapeutic platform for T1DM treatment.

#### 4. Conclusion

In summary, this study demonstrates a rapid and efficient method for forming Hislet using the FS device, significantly reducing the formation time from several days to few hours. By co-culturing dissociated pancreatic islet cells with ADSCs at an initial 1:1 ratio, we successfully generated stable spheroids with enhanced functionality. Co-culturing with ADSCs, known for their ECM synthesis properties, not only

facilitated stable spheroid formation but also endowed the Hislet with effective angiogenic and immunomodulatory properties. Importantly, Hislet maintained their primary function of glucose-responsive insulin secretion, even under conditions simulating the transplantation environment. Conventional approaches for forming p-islet aggregates typically rely on biomaterial scaffolds (e.g., collagen, agarose) or chemical modifications (e.g., magnetic beads), which introduce procedural complexity and potential safety risks, while still requiring prolonged culture times for p-islet formation (Supplementary Table 2) [15–18, 94–99]. In contrast, our FS device enables rapid physical aggregation of ADSCs and islet cells within hours via acoustic pressure, eliminating the need for exogenous materials or chemical agents. This method allows for the early establishment of critical cellular functions, including angiogenesis, insulin secretion, and immunomodulation. The rapid aggregation process has important clinical implications, as cell–cell connectivity is essential for optimal  $\beta$ -cell function and insulin secretion [100]. By applying this system, as supported by our data, we successfully shorten the time required for spheroid formation, generating Hislet that exhibit glucose-responsive insulin secretion within a significantly reduced timeframe. In conventional p-islet transplantation, persistent challenges such as insufficient angiogenesis at the graft site and immune cell-mediated attacks often result in graft failure, necessitating the use of systemic immunosuppressants [101]. However, immunosuppressive therapy is associated with increased risks of infection and other complications [102]. In contrast, Hislet inherently possess

immunomodulatory properties, which may reduce dependence on immunosuppressants and mitigate their associated risks. By addressing key limitations of conventional approaches, Hislet offer a promising and safer platform for more efficient clinical translation in islet transplantation therapy.

As a summary, the FS device-based ADSC co-culture approach addresses the drawbacks of prolonged culture time in traditional pseudo-islet formation and results in Hislet with higher survival potential upon transplantation. Collectively, FS device-based Hislet could offer a novel solution for treating T1DM by enhancing transplantation survival rates, holding promise for improving islet transplantation outcomes. However, before clinical application of ADSCs, further studies are required to evaluate potential risks previously associated with stem cell transplantation, such as unintended differentiation, tumorigenesis, dissociation from Hislet, and migration from the transplantation site [103]. These assessments should include long-term *in vivo* studies (over 90 days) using not only murine models but also medium-sized animal models such as pigs and dogs in order to evaluate the required Hislet does relative to increasing body weight.

#### CRediT authorship contribution statement

**Jiyu Hyun:** Writing – original draft, Visualization, Methodology, Formal analysis, Data curation, Conceptualization. **Junhyeung Park:** Validation, Investigation, Data curation. **Jihun Song:** Investigation, Data curation, Conceptualization. **Chaerim Yoo:** Methodology. **Seonmi Jang:** Methodology. **Sang Yoon Lee:** Validation, Investigation. **Jiseon An:** Formal analysis. **Hyun Su Park:** Data curation. **Seunghyuk Jung:** Formal analysis, Data curation. **Dasom Kong:** Methodology. **Ji Hyeon Cho:** Methodology. **Tae Il Lee:** Methodology, Investigation. **Ki Dong Park:** Writing – review & editing, Validation. **Gwang-Bum Im:** Data curation. **Jee-Heon Jeong:** Supervision, Data curation. **Hyun-Ji Park:** Writing – original draft, Software. **Dong Yun Lee:** Supervision, Funding acquisition, Conceptualization. **Suk Ho Bhang:** Writing – review & editing, Supervision, Resources, Project administration, Funding acquisition, Conceptualization.

#### Ethics approval and consent to participate

All animal experiments were conducted in strict accordance with national guidelines and received approval from the Institutional Animal Care and Use Committee (IACUC) of Sungkyunkwan University, South Korea (SKKUIACUC2023-01-31-1, and 2025-01-01-1).

#### Declaration of competing interests

The authors declare the following financial interests/personal relationships which may be considered as potential competing interests:

Ki Dong Park reports financial support was provided by Republic of Korea, Ministry of Trade, Industry & Energy. Jee-Heon Jeong reports financial support was provided by Republic of Korea, Ministry of Science and ICT. Hyun-Ji park reports financial support was provided by Republic of Korea, Ministry of Science and ICT and Ministry of Trade, Industry & Energy. Dong Yun Lee reports financial support was provided by Republic of Korea, Ministry of Science and ICT, the Ministry of Health & Welfare. Suk Ho Bhang reports financial support was provided by Republic of Korea, Ministry of Science and ICT, the Ministry of Health & Welfare and Ministry of Trade, Industry & Energy. Dong Yun Lee reports a relationship with Elixir Pharmatech Inc. That includes: employment. If there are other authors, they declare that they have no known competing financial interests or personal relationships that could have appeared to influence the work reported in this paper.

#### Acknowledgments

This work was supported by the National Research Foundation (NRF)

grants funded by the Ministry of Science and ICT (Grant No. RS-2023-00272815 to J-H.J., RS-2024-00411474 to H-J.P) and the Korean Fund for Regenerative Medicine (KFRM) grant funded by the Korea government (the Ministry of Science and ICT, the Ministry of Health & Welfare) (No. 21A0102L1-13 to S.H.B. and KFRM24A0105L1 to D.Y.L., Republic of Korea). This work also supported by the Alchemist Project of the Korea Evaluation Institute of Industrial Technology (KEIT 20018560, NTIS 2410005252 to S.H.B., H-J.P, and K.D.P), the Ministry of Trade, Industry & Energy, Republic of Korea.

#### Appendix A. Supplementary data

Supplementary data to this article can be found online at <https://doi.org/10.1016/j.bioactmat.2025.05.005>.

#### References

- [1] L.A. DiMeglio, C. Evans-Molina, R.A. Oram, Type 1 diabetes, *Lancet* 391 (10138) (2018) 2449–2462.
- [2] R.W. Beck, R.M. Bergenstal, L.M. Laffel, J.C. Pickup, Advances in technology for management of type 1 diabetes, *Lancet* 394 (10205) (2019) 1265–1273.
- [3] J.G. Joy, H.K. Son, S.-J. Lee, J.-C. Kim, Glucose-responsive soluble microneedle prepared with “Gelatin-hydroxyethylcellulose ethoxylate complex coacervate” for the transdermal drug delivery, *J. Ind. Eng. Chem.* 134 (2024) 432–447.
- [4] H. de Kort, E.J. de Koning, T.J. Rabelink, J.A. Bruijn, I.M. Bajema, Islet transplantation in type 1 diabetes, *Bmj* 342 (2011).
- [5] C. Ricordi, T.B. Strom, Clinical islet transplantation: advances and immunological challenges, *Nat. Rev. Immunol.* 4 (4) (2004) 259–268.
- [6] R. Lehmann, R.A. Zuellig, P. Kugelmeier, P.B. Baenninger, W. Moritz, A. Perren, P.-A. Clavien, M. Weber, G.A. Spinas, Superiority of small islets in human islet transplantation, *Diabetes* 56 (3) (2007) 594–603.
- [7] M. Brissova, A.C. Powers, Revascularization of transplanted islets: can it be improved? *Diabetes* 57 (9) (2008) 2269.
- [8] H. Li, Y. Shang, Q. Feng, Y. Liu, J. Chen, H. Dong, A novel bioartificial pancreas fabricated via islets microencapsulation in anti-adhesive core-shell microgels and macroencapsulation in a hydrogel scaffold prevascularized in vivo, *Bioact. Mater.* 27 (2023) 362–376.
- [9] S. Wu, L. Wang, Y. Fang, H. Huang, X. You, J. Wu, Advances in encapsulation and delivery strategies for islet transplantation, *Adv. Healthcare Mater.* 10 (20) (2021) 2100965.
- [10] D. Rojas-Canales, S.N. Walters, D. Penko, D. Cultrone, J. Bailey, T. Chtanova, J. Nitschke, J. Johnston, S. Kireta, T. Loudovaris, Intracutaneous transplantation of islets within a biodegradable temporizing matrix as an alternative site for islet transplantation, *Diabetes* 72 (6) (2023) 758–768.
- [11] N. Kasoji, A. Pátíková, E. Wawrzynska, A. Vojtíšková, T. Sedláček, M. Kumorek, O. Pop-Georgievski, E. Sticová, J. Kríž, D. Kubies, Bioengineering a pre-vascularized pouch for subsequent islet transplantation using VEGF-loaded polylactide capsules, *Biomater. Sci.* 8 (2) (2020) 631–647.
- [12] A. Ershad-Langroudi, N. Babazadeh, F. Alizadeh, S.M. Mousaei, G. Moradi, Polymers for implantable devices, *J. Ind. Eng. Chem.* 137 (25) (2024) 61–86.
- [13] C. Bildeau, O. Goltsis, I.M. Rogers, M. Post, Limitations of recellularized biological scaffolds for human transplantation, *J. Tissue Eng. Regen. Med.* 14 (3) (2020) 521–538.
- [14] D. Zorzi, T. Phan, M. Sequi, Y. Lin, D.H. Freeman, L. Cicalese, C. Castellini, Impact of islet size on pancreatic islet transplantation and potential interventions to improve outcome, *Cell Transplant.* 24 (1) (2015) 11–23.
- [15] S. Pathak, S. Regmi, B. Gupta, T.T. Pham, C.S. Yong, J.O. Kim, S. Yook, J.R. Kim, M.H. Park, Y.K. Bae, Engineered islet cell clusters transplanted into subcutaneous space are superior to pancreatic islets in diabetes, *FASEB J.* 31 (11) (2017) 5111–5121.
- [16] E. Lorz-Gil, F. Gerst, M.B. Oquendo, U. Deschl, H.-U. Häring, M. Beilmann, S. Ullrich, Glucose, adrenaline and palmitate antagonistically regulate insulin and glucagon secretion in human pseudoislets, *Sci. Rep.* 9 (1) (2019) 10261.
- [17] M. Urbanczyk, A. Zbinden, S.L. Layland, G. Duffy, K. Schenke-Layland, Controlled heterotypic pseudo-islet assembly of human  $\beta$ -cells and human umbilical vein endothelial cells using magnetic levitation, *Tissue Eng.* 26 (7–8) (2020) 387–399.
- [18] A.E. Vlahos, S.M. Kinney, B.R. Kingston, S. Keshavjee, S.-Y. Won, A. Martyts, W. C. Chan, M.V. Sefton, Endothelialized collagen based pseudo-islets enables tuneable subcutaneous diabetes therapy, *Biomaterials* 232 (2020) 119710.
- [19] R. MacGregor, S. Williams, P. Tong, K. Kover, W. Moore, L. Stehno-Bittel, Small rat islets are superior to large islets in *in vitro* function and in transplantation outcomes, *Am. J. Physiol. Endocrinol. Metabol.* 290 (5) (2006) E771–E779.
- [20] N. Sakata, M. Goto, G. Yoshimatsu, S. Egawa, M. Unno, Utility of co-transplanting mesenchymal stem cells in islet transplantation, *World J. Gastroenterol.* 17 (47) (2011) 5150.
- [21] M. Sui, T. Li, H. Lu, Y. Li, J. Huang, P. Zhang, S. Wang, L. Zeng, SOCS3 inhibits the mesenchymal stromal cell secretory factor SDF-1-mediated improvement of islet function in non-obese diabetic mice, *Stem Cell Res. Ther.* 14 (1) (2023) 172.
- [22] S. Keshkar, M. Kaviani, F.S. Sarvestani, M.H. Ghahremani, M.H. Aghdai, I.H. Al-Abdullah, N. Azarpira, Exosomes derived from human mesenchymal stem cells



- preserve mouse islet survival and insulin secretion function, *EXCLI J.* 19 (2020) 1064.
- [23] E. Montanari, R.P. Meier, R. Mahou, J.D. Seebach, C. Wandrey, S. Gerber-Lemaire, L.H. Buhler, C. Gonelle-Gispert, Multipotent mesenchymal stromal cells enhance insulin secretion from human islets via N-cadherin interaction and prolong function of transplanted encapsulated islets in mice, *Stem Cell Res. Ther.* 8 (2017) 1–12.
  - [24] M.S. Friedlander, V.M. Nguyen, S.K. Kim, R.J. Bevacqua, Pancreatic pseudoislets: an organoid archetype for metabolism research, *Diabetes* 70 (5) (2021) 1051–1060.
  - [25] F.C. Wieland, M.M. Stijhs, T. Geuens, C.A. van Blitterswijk, V.L. LaPointe, The role of alpha cells in the self-assembly of bioengineered islets, *Tissue Eng.* 27 (15–16) (2021) 1055–1063.
  - [26] G.B. Im, Y.J. Kim, T.I. Lee, S.H. Bhang, Subaqueous free-standing 3D cell culture system for ultrafast cell compaction, mechano-inductive immune control, and improving therapeutic angiogenesis, *Bioeng.* Trans. Med. 8 (2) (2023) e10438.
  - [27] J.M. Gimble, A.J. Katz, B.A. Bunnell, Adipose-derived stem cells for regenerative medicine, *Circ. Res.* 100 (9) (2007) 1249–1260.
  - [28] S. Al-Ghadban, B.A. Bunnell, Adipose tissue-derived stem cells: immunomodulatory effects and therapeutic potential, *Physiology* 35 (2) (2020) 125–133.
  - [29] O.I. Badr, A. Anter, I. Magdy, M. Chukueggu, M. Khorshid, M. Darwish, M. Farrag, M. Elsayed, Y. Amr, Y. Amgad, Adipose-derived mesenchymal stem cells and their derived epidermal progenitor cells conditioned media ameliorate skin aging in rats, *Tissue Eng. Regen. Med.* 21 (6) (2024) 915–927.
  - [30] S.H. Bhang, S.-W. Cho, W.-G. La, T.-J. Lee, H.S. Yang, A.-Y. Sun, S.-H. Baek, J.-W. Rhie, B.-S. Kim, Angiogenesis in ischemic tissue produced by spheroid grafting of human adipose-derived stromal cells, *Biomaterials* 32 (11) (2011) 2734–2747.
  - [31] Y. Kang, J. Na, G. Karima, S. Amirthalingam, N.S. Hwang, H.D. Kim, Mesenchymal stem cell spheroids: a promising tool for vascularized tissue regeneration, *Tissue Eng. Regen. Med.* 21 (5) (2024) 673–693.
  - [32] S. Kang, S.M. Kim, J.H. Sung, Cellular and molecular stimulation of adipose-derived stem cells under hypoxia, *Cell Biol. Int.* 38 (5) (2014) 553–562.
  - [33] J. Xu, X. Liu, F. Zhao, Y. Zhang, Z. Wang, HIF1 $\alpha$  overexpression enhances diabetic wound closure in high glucose and low oxygen conditions by promoting adipose-derived stem cell paracrine function and survival, *Stem Cell Res. Ther.* 11 (2020) 1–13.
  - [34] M. Marinkovic, O.N. Tran, T.J. Block, R. Rakian, A.O. Gonzalez, D.D. Dean, C.-K. Yeh, X.-D. Chen, Native extracellular matrix, synthesized ex vivo by bone marrow or adipose stromal cells, faithfully directs mesenchymal stem cell differentiation, *Matrix Biol.* 8 (2020) 100044.
  - [35] T. Gonzalez-Fernandez, A.J. Tenorio, A.M. Saiz Jr., J.K. Leach, Engineered cell-secreted extracellular matrix modulates cell spheroid mechanosensing and amplifies their response to inductive cues for the formation of mineralized tissues, *Adv. Healthcare Mater.* 11 (10) (2022) 2102337.
  - [36] Y. Li, X. Ding, X. Tian, J. Zheng, C. Ding, X. Li, X. Hu, Y. Qiao, Y. Wang, W. Xue, Islet transplantation modulates macrophage to induce immune tolerance and angiogenesis of islet tissue in type I diabetes mice model, *Aging (Albany NY)* 12 (23) (2020) 24023.
  - [37] B.M. de Souza, A.P. Boucas, F.d.S.d. Oliveira, K.P. Reis, P. Ziegelmann, A. C. Bauer, D. Crispim, Effect of co-culture of mesenchymal stem/stromal cells with pancreatic islets on viability and function outcomes: a systematic review and meta-analysis, *Islets* 9 (2) (2017) 30–42.
  - [38] M.J. Kim, Y. Lee, S. Jon, D.Y. Lee, PEGylated bilirubin nanoparticle as an anti-oxidative and anti-inflammatory demulcent in pancreatic islet xenotransplantation, *Biomaterials* 133 (2017) 242–252.
  - [39] P. Buchwald, X. Wang, A. Khan, A. Bernal, C. Fraker, L. Invernardi, C. Ricordi, Quantitative assessment of islet cell products: estimating the accuracy of the existing protocol and accounting for islet size distribution, *Cell Transplant.* 18 (10–11) (2009) 1223–1235.
  - [40] E.V. Koudan, A.A. Gryadunova, P.A. Karalkin, J.V. Korneva, N.Y. Meteleva, I. I. Babichenko, A.V. Volkov, S.A. Rodionov, V.A. Parfenov, F.D. Pereira, Multiparametric analysis of tissue spheroids fabricated from different types of cells, *Biotechnol. J.* 15 (5) (2020) 1900217.
  - [41] G.-B. Im, S.-W. Kim, S.H. Bhang, Fortifying the angiogenic efficacy of adipose derived stem cell spheroids using spheroid compaction, *J. Ind. Eng. Chem.* 93 (2021) 228–236.
  - [42] M. Cavo, D. Delle Cave, E. D'Amone, G. Gigli, E. Leonardo, L.L. Del Mercato, A synergic approach to enhance long-term culture and manipulation of MiaPaCa-2 pancreatic cancer spheroids, *Sci. Rep.* 10 (1) (2020) 10192.
  - [43] D. Foresti, M. Nabavi, M. Klingauf, A. Ferrari, D. Poulikakos, Acoustophoretic contactless transport and handling of matter in air, *Proc. Natl. Acad. Sci.* 110 (31) (2013) 12549–12554.
  - [44] C. Pardo-Pastor, F. Rubio-Moscardo, M. Vogel-González, S.A. Serra, A. Afthinos, S. Mrkonjic, O. Destaig, J.F. Abenza, J.M. Fernández-Fernández, X. Trepast, Piezo2 channel regulates RhoA and actin cytoskeleton to promote cell mechanobiological responses, *Proc. Natl. Acad. Sci.* 115 (8) (2018) 1925–1930.
  - [45] N. Braidotti, S.N. Chen, C.S. Long, D. Cojoc, O. Sbaizero, Piezo1 channel as a potential target for hindering cardiac fibrotic remodeling, *Int. J. Mol. Sci.* 23 (15) (2022) 8065.
  - [46] F. Tao, K. Sayo, K. Sugimoto, S. Aoki, N. Kojima, Development of a tunable method to generate various three-dimensional microstructures by replenishing macromolecules such as extracellular matrix components and polysaccharides, *Sci. Rep.* 10 (1) (2020) 6567.
  - [47] K.K. Yap, A.M. Dingle, J.A. Palmer, R.S. Dhillon, Z. Lokmic, A.J. Penington, G. C. Yeoh, W.A. Morrison, G.M. Mitchell, Enhanced liver progenitor cell survival and differentiation in vivo by spheroid implantation in a vascularized tissue engineering chamber, *Biomaterials* 34 (16) (2013) 3992–4001.
  - [48] H. Komatsu, C. Cook, C.-H. Wang, L. Medrano, H. Lin, F. Kandeel, Y.-C. Tai, Y. Mullen, Oxygen environment and islet size are the primary limiting factors of isolated pancreatic islet survival, *PLoS One* 12 (8) (2017) e0183780.
  - [49] W. Li, R. Zhao, J. Liu, M. Tian, Y. Lu, T. He, M. Cheng, K. Liang, X. Li, X. Wang, Small islets transplantation superiority to large ones: implications from islet microcirculation and revascularization, *J. Diabetes Res.* 2014 (1) (2014) 192093.
  - [50] T. Tanaka, D. Kojima, T. Mera, M. Matsumoto, Y. Yasunami, T. Yanase, Expansion of transplanted islets in mice by co-transplantation with adipose tissue-derived mesenchymal stem cells, *Heliyon* 4 (5) (2018) e00632.
  - [51] C. Frantz, K.M. Stewart, V.M. Weaver, The extracellular matrix at a glance, *J. Cell Sci.* 123 (24) (2010) 4195–4200.
  - [52] T. Martins-Marques, T. Ribeiro-Rodrigues, D. Batista-Almeida, T. Aasen, B. R. Kwak, H. Girao, Biological functions of connexin43 beyond intercellular communication, *Trends Cell Biol.* 29 (10) (2019) 835–847.
  - [53] F. Van Roy, G. Berx, The cell-cell adhesion molecule E-cadherin, *Cell. Mol. Life Sci.* 65 (2008) 3756–3788.
  - [54] G. Gui, J. Puddfoot, G. Vinson, C. Wells, R. Carpenter, In vitro regulation of human breast cancer cell adhesion and invasion via integrin receptors to the extracellular matrix, *Br. J. Surg.* 82 (9) (1995) 1192–1196.
  - [55] L.M. Weber, K.N. Hayda, K.S. Anseth, Cell-matrix interactions improve  $\beta$ -cell survival and insulin secretion in three-dimensional culture, *Tissue Eng.* 14 (12) (2008) 1959–1968.
  - [56] L.A. Liacua, M.M. Faas, P. de Vos, Extracellular matrix molecules and their potential contribution to the function of transplanted pancreatic islets, *Diabetologia* 61 (2018) 1261–1272.
  - [57] D.T. Bowers, W. Song, L.-H. Wang, M. Ma, Engineering the vasculature for islet transplantation, *Acta Biomater.* 95 (2019) 131–151.
  - [58] N. Ferrara, The role of VEGF in the regulation of physiological and pathological angiogenesis. Mechanisms of Angiogenesis, 2005, pp. 209–231.
  - [59] S. Shigematsu, K. Yamauchi, K. Nakajima, S. Iijima, T. Aizawa, K. Hashizume, IGF-1 regulates migration and angiogenesis of human endothelial cells, *Endocr. J.* 46 (Suppl) (1999) S59–S62.
  - [60] M. Rizov, P. Andreeva, I. Dimova, Molecular regulation and role of angiogenesis in reproduction, *Taiwan. J. Obstet. Gynecol.* 56 (2) (2017) 127–132.
  - [61] R.J. Aviles, B.H. Annex, R.J. Lederman, Testing clinical therapeutic angiogenesis using basic fibroblast growth factor (FGF-2), *Br. J. Pharmacol.* 140 (4) (2003) 637–646.
  - [62] M. Bakhti, A. Böttcher, H. Lickert, Modelling the endocrine pancreas in health and disease, *Nat. Rev. Endocrinol.* 15 (3) (2019) 155–171.
  - [63] M. Brissova, A. Shostak, M. Shiota, P.O. Wiebe, G. Poffenberger, J. Kantz, Z. Chen, C. Carr, W.G. Jerome, J. Chen, Pancreatic islet production of vascular endothelial growth factor- $\alpha$  is essential for islet vascularization, revascularization, and function, *Diabetes* 55 (11) (2006) 2974–2985.
  - [64] F. Waldron-Lynch, K.C. Herold, Immunomodulatory therapy to preserve pancreatic  $\beta$ -cell function in type 1 diabetes, *Nat. Rev. Drug Discov.* 10 (6) (2011) 439–452.
  - [65] C. Trotzier, C. Bellanger, H. Abdessadeq, P. Delannoy, A. Mojallal, C. Auxenfans, Deciphering influence of donor age on adipose-derived stem cells: in vitro paracrine function and angiogenic potential, *Sci. Rep.* 14 (1) (2024) 27589.
  - [66] B. Qi, Y. Ding, Y. Zhang, L. Kou, Y.-Z. Zhao, Q. Yao, Biomaterial-assisted strategies to improve islet graft revascularization and transplant outcomes, *Biomater. Sci.* 12 (4) (2024) 821–836.
  - [67] K. Fujimoto, K.S. Polonsky, Pdx1 and other factors that regulate pancreatic  $\beta$ -cell survival, *Diabetes, Obes. Metabol.* 11 (2009) 30–37.
  - [68] A.A. Mamun, H. Hayashi, A. Yamamura, M.J. Nayeem, M. Sato, Hypoxia induces the translocation of glucose transporter 1 to the plasma membrane in vascular endothelial cells, *J. Physiol. Sci.* 70 (2020) 1–15.
  - [69] C.-Y. Zhang, G. Baffy, P. Perret, S. Krauss, O. Peroni, D. Grujic, T. Hagen, A. J. Vidal-Puig, O. Boss, Y.-B. Kim, Uncoupling protein-2 negatively regulates insulin secretion and is a major link between obesity,  $\beta$  cell dysfunction, and type 2 diabetes, *Cell* 105 (6) (2001) 745–755.
  - [70] C.T. DeSouza, E.P. Araújo, L.F. Stoppiglia, J.R. Pauli, E. Ropelle, S.A. Rocco, R. M. Marin, K.G. Franchini, J.B. Carvalheira, M.J. Saad, Inhibition of UCP2 expression reverses diet-induced diabetes mellitus by effects on both insulin secretion and action, *FASEB J.* 21 (4) (2007) 1153–1163.
  - [71] A. Mildmay-White, W. Khan, Cell surface markers on adipose-derived stem cells: a systematic review, *Curr. Stem Cell Res. Ther.* 12 (6) (2017) 484–492.
  - [72] P. Hansell, W.J. Welch, R.C. Blantz, F. Palm, Determinants of kidney oxygen consumption and their relationship to tissue oxygen tension in diabetes and hypertension, *Clin. Exp. Pharmacol. Physiol.* 40 (2) (2013) 123–137.
  - [73] A. Gamble, A. Pepper, A. Bruni, A. Shapiro, The journey of islet cell transplantation and future development, *Islets* 10 (2018) 80–94.
  - [74] L. Jansson, P.-O. Carlsson, Graft vascular function after transplantation of pancreatic islets, *Diabetologia* 45 (2002) 749–763.
  - [75] L. Buravkova, E. Andreeva, V. Gogvadze, B. Zhivotovskiy, Mesenchymal stem cells and hypoxia: where are we? *Mitochondrion* 19 (2014) 105–112.
  - [76] T. Gao, B. McKenna, C. Li, M. Reichert, J. Nguyen, T. Singh, C. Yang, A. Pannikar, N. Doliba, T. Zhang, Pdx1 maintains  $\beta$  cell identity and function by repressing an  $\alpha$  cell program, *Cell Metab.* 19 (2) (2014) 259–271.
  - [77] M.A. Kanak, M. Takita, F. Kunnathodi, M.C. Lawrence, M.F. Levy, B. Naziruddin, Inflammatory response in islet transplantation, *Int. J. Endocrinol.* 2014 (1) (2014) 451035.
  - [78] M.H. Oberbarnscheidt, D. Zecher, F.G. Lakkis, The innate immune system in transplantation, in: *Seminars in Immunology*, Elsevier, 2011, pp. 264–272.



- [79] S.E. Panzer, Macrophages in transplantation: a matter of plasticity, polarization, and diversity, *Transplantation* 106 (2) (2022) 257–267.
- [80] X. Shao, Roles of M1 and M2 macrophage infiltration in post-renal transplant antibody-mediated rejection, *Transpl. Immunol.* 85 (2024) 102076.
- [81] T.A. Wynn, K.M. Vannella, Macrophages in tissue repair, regeneration, and fibrosis, *Immunity* 44 (3) (2016) 450–462.
- [82] J.A. Hutchinson, Macrophages in transplantation, *Transplantation* 99 (5) (2015) 898–899.
- [83] W. Gou, W. Hua, L. Swaby, W. Cui, E. Green, K.A. Morgan, C. Strange, H. Wang, Stem cell therapy improves human islet graft survival in mice via regulation of macrophages, *Diabetes* 71 (12) (2022) 2642–2655.
- [84] J.A. Trapani, M.J. Smyth, Functional significance of the perforin/granzyme cell death pathway, *Nat. Rev. Immunol.* 2 (10) (2002) 735–747.
- [85] M. Romano, S.L. Tung, L.A. Smyth, G. Lombardi, Treg therapy in transplantation: a general overview, *Transpl. Int.* 30 (8) (2017) 745–753.
- [86] Y. Chen, J. Chen, Z. Liu, S. Liang, X. Luan, F. Long, Y. Peng, L. Yan, J. Gong, Relationship between TH1/TH2 cytokines and immune tolerance in liver transplantation in rats, in: *Transplantation Proceedings*, Elsevier, 2008, pp. 2691–2695.
- [87] A. Kanhere, A. Hertweck, U. Bhatia, M.R. Gökmen, E. Perucha, I. Jackson, G. M. Lord, R.G. Jenner, T-bet and GATA3 orchestrate Th1 and Th2 differentiation through lineage-specific targeting of distal regulatory elements, *Nat. Commun.* 3 (1) (2012) 1268.
- [88] J. Mariotti, J. Foley, K. Ryan, N. Buxhoeveden, V. Kapoor, S. Amarnath, D. H. Fowler, Graft rejection as a Th1-type process amenable to regulation by donor Th2-type cells through an interleukin-4/STAT6 pathway, *Blood, J. Am. Soc. Hematol.* 112 (12) (2008) 4765–4775.
- [89] A. Kroemer, X. Xiao, N. Degauque, K. Edtinger, H. Wei, G. Demirci, X.C. Li, The innate NK cells, allograft rejection, and a key role for IL-15, *J. Immunol.* 180 (12) (2008) 7818–7826.
- [90] V. Zarkhin, G. Chalasani, M.M. Sarwal, The yin and yang of B cells in graft rejection and tolerance, *Transplant. Rev.* 24 (2) (2010) 67–78.
- [91] D. Schmidt, A. Von Hochstetter, The use of CD31 and collagen IV as vascular markers a study of 56 vascular lesions, *Pathol. Res. Pract.* 191 (5) (1995) 410–414.
- [92] O.C. Richards, S.M. Raines, A.D. Attie, The role of blood vessels, endothelial cells, and vascular pericytes in insulin secretion and peripheral insulin action, *Endocr. Rev.* 31 (3) (2010) 343–363.
- [93] A.R. Pepper, B. Gala-Lopez, O. Ziff, A.J. Shapiro, Revascularization of transplanted pancreatic islets and role of the transplantation site, *J. Immunol. Res.* 2013 (1) (2013) 352315.
- [94] Y. Ichihara, R. Utoh, M. Yamada, T. Shimizu, Y. Uchigata, Size effect of engineered islets prepared using microfabricated wells on islet cell function and arrangement, *Heliyon* 2 (6) (2016) e00129.
- [95] J. Hilderink, S. Spijker, F. Carlotti, L. Lange, M. Engelse, C. van Blitterswijk, E. de Koning, M. Karperien, A. van Apeldoorn, Controlled aggregation of primary human pancreatic islet cells leads to glucose-responsive pseudoislets comparable to native islets, *J. Cell Mol. Med.* 19 (8) (2015) 1836–1846.
- [96] A. Rubio-Navarro, N. Gómez-Banoy, L. Stoll, F. Dünder, A.M. Mawla, L. Ma, E. Cortada, P. Zumbo, A. Li, M. Reiterer, A beta cell subset with enhanced insulin secretion and glucose metabolism is reduced in type 2 diabetes, *Nat. Cell Biol.* 25 (4) (2023) 565–578.
- [97] U. Johansson, N.D. Shalaly, L.C. Hjelm, M. Ria, P.-O. Berggren, M. Hedhammar, Integration of primary endocrine cells and supportive cells using functionalized silk promotes the formation of prevascularized islet-like clusters, *ACS Biomater. Sci. Eng.* 6 (2) (2019) 1186–1195.
- [98] J.T. Walker, R. Haliyur, H.A. Nelson, M. Ishahak, G. Poffenberger, R. Aramandla, C. Reihsmann, J.R. Luchsinger, D.C. Saunders, P. Wang, Integrated human pseudoislet system and microfluidic platform demonstrate differences in GPCR signaling in islet cells, *JCI insight* 5 (10) (2020) e137017.
- [99] R.J. Bevacqua, X. Dai, J.Y. Lam, X. Gu, M.S. Friedlander, K. Tellez, I. Miguel-Escalada, S. Bonàs-Guarch, G. Atla, W. Zhao, CRISPR-based genome editing in primary human pancreatic islet cells, *Nat. Commun.* 12 (1) (2021) 2397.
- [100] K.M. Shekro, T.H. Hraha, A.B. Bernard, R.K. Benninger, K.S. Anseth, Engineering functional pseudo-islets of defined sizes from primary murine cells using PEG microwell devices, *bioRxiv* (2020), 2020.02. 07.939538.
- [101] S.A. Nanji, A.J. Shapiro, Islet transplantation in patients with diabetes mellitus: choice of immunosuppression, *BioDrugs* 18 (2004) 315–328.
- [102] A. Buxeda, D. Redondo-Pachón, M.J. Pérez-Sáez, M. Crespo, J. Pascual, Sex differences in cancer risk and outcomes after kidney transplantation, *Transplant. Rev.* 35 (3) (2021) 100625.
- [103] B. Lukomska, L. Stanaszek, E. Zuba-Surma, P. Legosz, S. Sarzynska, K. Dreła, Challenges and controversies in human mesenchymal stem cell therapy, *Stem Cell. Int.* 2019 (1) (2019) 9628536.